Pillar[5]arene-Decorated Single-Walled Carbon Nanotubes

PILLAR[5]ARENE-DECORATED SINGLE-WALLED CARBON

NANOTUBES

BY

CHRISTINA SHAMSHOOM, B.Sc.

A THESIS

SUBMITTED TO THE DEPARTMENT OF CHEMISTRY AND CHEMICAL BIOLOGY

AND THE SCHOOL OF GRADUATE STUDIES

OF McMASTER UNIVERSITY

IN PARTIAL FULFILMENT OF THE REQUIREMENTS

FOR THE DEGREE OF

M.Sc. IN CHEMISTRY

MSc of Chemistry (2018)   McMaster University

(Chemistry and Chemical Biology)   Hamilton, Ontario, Canada

TITLE: Pillar[5]arene-Decorated Single-Walled Carbon Nanotubes

AUTHOR: Christina Shamshoom

       B.Sc., (Chemistry)

       University of Guelph, Guelph, Canada

SUPERVISOR: Professor Alex Adronov

NUMBER OF PAGES: ix, 89

Abstract

Control of single-walled carbon nanotube dispersion properties is of substantial interest to the scientific community. In this work, we sought to investigate the effect of a macrocycle, the pillar[5]arene, on the dispersion properties of a polymer-nanotube complex. Pillar[5]arenes are a class of electron-rich macrocyclic hosts capable of forming inclusion complexes with electron-poor guests, such as alkyl nitriles. A hydroxyl-functionalized pillar[5]arene derivative was coupled to the alkyl bromide side-chains of a polyfluorene, which was then used to coat the surface of single-walled carbon nanotubes. Differentiation of semiconducting and metallic SWNT species was analyzed by a combination of UV-Vis-NIR, Raman, and fluorescence spectroscopy. Raman spectroscopy confirmed that the concentrated nanotube dispersion produced by the macrocycle-containing polymer was due to well-exfoliated nanotubes, rather than bundle formation. The polymer-nanotube dispersion was investigated using ^{1}H-NMR spectroscopy, and it was found that host-guest chemistry between pillar[5]arene and 1,6-dicyanohexane occurred in the presence of the polymer-nanotube complex. Utilizing the host-guest capability of pillar[5]arene, the polymer-nanotube complex was incorporated into a supramolecular organogel.

Acknowledgements

Throughout my M.Sc. degree, I have had the opportunity to work with numerous individuals who have helped me to achieve my academic goals. First, I would like to thank my academic supervisor Dr. Alex Adronov for taking me on as a student and guiding me throughout my degree. Under your supervision, I gained immense scientific knowledge and valuable research experience that I will take with me as I move forward in my career. Also, I would like to thank my supervisory committee, Dr. Ryan Wylie and Dr. Harald Stöver for their suggestions and helpful discussions.

The following thesis would not have been possible without the help of numerous individuals in the Adronov group: Dr. Nicole Rice, Stuart McNelles, Vladimir Kardelis, Darryl Fong, Kelvin Li, William J. Bodnaryk, and Dr. Eric Meichsner. I am truly indebted to all of you for the training, support, and guidance you offered over the past two years. I will always cherish the laughter, fun times, and comradery we shared. It has been a pleasure getting to know all of you and working alongside you in lab. Thank you for being there for me when my experiments did not work and offering advice despite your busy schedules.

Most importantly, I would like to express my deep gratitude towards my parents and siblings for their endless support and unconditional love. You have been truly instrumental in all my achievements, and without you, my university degrees would not have been possible.

Table of Contents

List of Figures

List of Schemes

Chapter 1: Introduction

1.1. Introduction to Carbon Nanotubes

Immediately following the synthesis of fullerenes on a macroscopic scale,[1] the Japanese physicist Sumio Iijima accidentally discovered carbon nanotubes on the surface of graphite electrodes used in an electric arc discharge.[2] Carbon nanotubes are hollow, tubular allotropes of carbon that are approximately 1 nm in diameter and roughly 1 µm in length.[3] As shown in Figure 1, carbon nanotubes may be composed of one layer of carbon atoms to form a single-walled carbon nanotube (SWNT), or multiple SWNTs of different diameters placed inside one another to form a multi-walled carbon nanotube (MWNT). Since their discovery in 1993,[2] single-walled carbon nanotubes (SWNTs) have attracted significant interest within the scientific community because of their extraordinary structural,[4–6] mechanical,[7–9] and optoelectronic properties.[10–12]
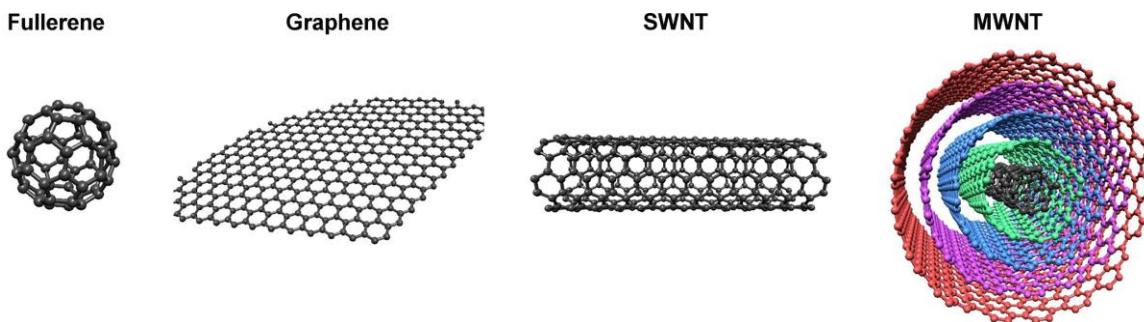
Figure 1. Various examples of carbon allotropes. Adapted from [Rice, N. A. Separation of Single-Walled Carbon Nanotubes By Electronic Type Using Conjugated Polymers, McMaster University, 2015].[13]

Theoretically, SWNTs can be imagined as a graphene sheet that is rolled up to form a cylinder, as shown in Figure 2. The different permutations of the two-dimensional "rolled up" graphene lattice generates an assortment of quasi-one-dimensional nanotube species such as zigzag, armchair, and helical (commonly known as chiral) SWNTs.[14] The

numerous ways in which a graphene sheet is rolled into a carbon nanotube may be defined

mathematically by the chiral vector equation:

$$C_h = na_1 + ma_2 = d_t \pi \qquad (1)$$

Where n and m are integers which correspond to the lattice translational indices,

and a_1 and a_2 are unit vectors for the graphene lattice (Figure 2). The chiral vector is also

related to the SWNT diameter (d_t) because it encompasses the circumference of the rolled-

up nanotube.[14] Carbon nanotubes are also described by the chiral angle, θ, which is defined

as the angle between the vectors C_h and a_1 as shown by the following equation:

$$\theta = tan^{-1} \left[\frac{\sqrt{3m}}{(2n+m)} \right] \qquad (2)$$

The values of chiral angle are restricted to $0 - 30°$ due to the hexagonal symmetry

of the graphene lattice. The values on either extreme of the range (i.e. $0°$ and $30°$) are

present in achiral SWNTs. Thus, a given nanotube is zigzag if $\theta = 0°$ ($m = 0$), while if $\theta =$

$30°$ ($n = m$) it is known as an armchair SWNT. As shown in Figure 2, having a chiral vector

perpendicular to the C=C bond directions (shown in blue) will generate a zigzag SWNT,

denoted as ($n, 0$).[14] Conversely, if the chiral vector is parallel to the direction of the C=C

bond (shown in red), it will result in an armchair SWNT.[14] The chiral angle values in

between 0 and $30°$ are present in chiral SWNTs that lack mirror symmetry.
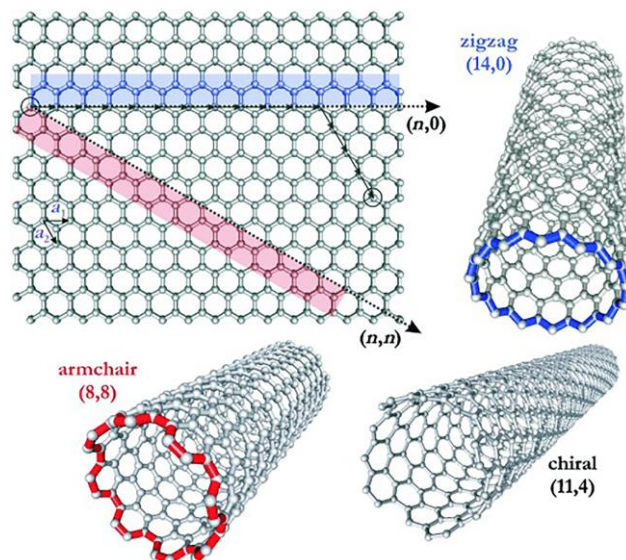
Figure 2. The "roll-up" of a graphene sheet which generates zigzag (blue), armchair (red), and chiral (gray) SWNTs. Reproduced with permission from [Balasubramanian, K.; Burghard, M. *Small* **2005**, *1* (2), 180–192].[15] Copyright John Wiley & Sons, 2004.

1.1.1. Synthesis of Carbon Nanotubes

Commercial carbon nanotubes are synthesized by various techniques, including arc discharge, laser ablation, chemical vapor deposition (CVD), high-pressure carbon monoxide disproportionation (HiPCO), and a CVD variant that uses a cobalt-molybdenum catalyst called CoMoCAT.[16] In 1991, Iijima reported the first synthesis of carbon nanotubes (MWNTs) *via* an arc discharge evaporation method, similar to fullerene synthesis.[2] The resultant needle-like tubes were approximately 4 to 30 nm in diameter and about 1 µm in length.[2] The carbon nanotubes were grown on the negative end of a carbon electrode inside a pressurized chamber composed of a mixture of methane and argon gas, at pressures of 10 Torr and 40 Torr, respectively. Inside the pressurized chamber, a current was applied across a metal catalyst-impregnated cathode and electrode, resulting in carbon

nanotubes that grew on the catalyst particles.[17] Hence, arc-discharge evaporation is the oldest reported method used for fabrication of carbon nanotubes in macroscopic amounts.[2]

Another method for the bulk synthesis of SWNTs, known as laser ablation, was first introduced by Smalley and co-workers in 1995.[18] It involves direct laser vaporization of a transition metal-graphite target in a high temperature reactor that contains an inert gas.[18] The gas phase carbon rises and as it reaches the cold surface of the reactor walls, the carbon condenses to grow carbon nanotubes. While the fundamental nanotube growth mechanism is akin to the arc-discharge method, direct vaporization has some advantages such as improved control over growth conditions and it efficiently generates nanotubes in higher yield (up to 70%).[18] In addition, the laser ablation method affords more control in the diameter of the carbon nanotubes synthesized.[19]

CVD is another synthetic method of carbon nanotubes which was developed by Xie and co-workers in 1996.[20] This method involves the catalytic decomposition of a hydrocarbon gas (such as methane, ethene and ethyne) on a solid catalyst in a high temperature (700 to 900°C) chamber.

The HiPCO method was first developed by researchers at Rice University in 1999, where carbon nanotubes are synthesized in a high pressure and high temperature (700 to 900°C) chamber. It is a scalable, continuous process which generates sizeable amounts of SWNTs formed free of a catalyst support. This method is similar to CVD, with the exception that the catalyst is introduced in the gas phase as opposed to the solid state. The HiPCO method utilizes carbon monoxide gas as a carbon source and iron pentacarbonyl

$(Fe(CO)_5)$ catalyst, where the iron forms metal clusters that act as catalytic sites on which small diameter carbon nanotubes (0.7 to 1.3 nm) grow.[21]

The CoMoCAT process also involves the disproportionation of carbon monoxide gas, however the carbon nanotubes are grown on a special cobalt-molybdenum (CoMo) catalyst.[22] In a high temperature (700–950°C) chamber, the pure carbon monoxide gas is introduced at a total pressure that typically ranges from 1 to 10 atm.[22] The CoMoCAT process generates a large amount of nanotube material, with over 80% of SWNTs grown by this method.

1.2. Solubilization of Carbon Nanotube Bundles

Carbon nanotubes form bundles due to the presence of strong intermolecular forces such as van der Waals and π–π stacking, as shown in Figure 3.[3] The entangled bundles are insoluble in all organic solvents and aqueous media.[3] While it is possible to disperse carbon nanotubes in some solvents through vigorous sonication, they immediately aggregate and re-form bundles when the sonication process is momentarily halted.[3] Due to their lack of solubility in any solvents, the use and applications of carbon nanotubes are generally limited. As previously discussed, commercial SWNT synthetic methods result in a complex mixture of semiconducting and metallic SWNTs, as well as amorphous carbon and metal catalyst particles.[23–27] As a result, significant research toward the solubilization of carbon nanotubes is currently under investigation. Mainly, covalent and noncovalent functionalization methods have been extensively studied and employed for the solubilization of carbon nanotubes.[28–30]
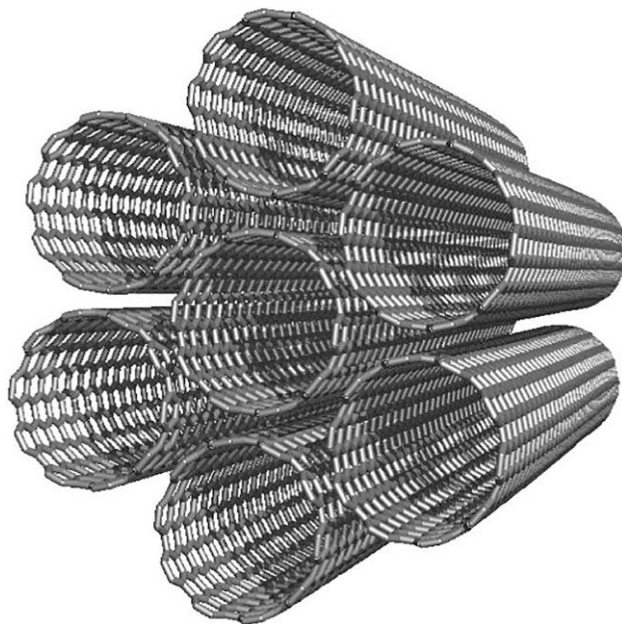
Figure 3. Idealized representation of SWNTs in a bundle. Reproduced with permission from [Hirsch, A. *Angew. Chemie - Int. Ed.* **2002**, *41* (11), 1853–1859].[30] Copyright John Wiley & Sons, 2002.

1.2.1. Covalent Functionalization of SWNTs

Some of the first accounts of covalent chemistry on SWNTs involve ultrasonication of a mixture of concentrated nitric and sulfuric acid to introduce oxygenated functional groups (such as carboxylic acids) at the ends and at defects on the sidewalls of carbon nanotubes.[15] The resultant carboxyl groups enable further functionalization through amidation or esterification to introduce various groups onto the SWNTs.[15] Covalent decoration of nanotube sidewalls has also been achieved using a variety of reactive reagents, such as carbenes, nitrenes, and radicals, which have enabled introduction of many different functionalities on the nanotube surface.[3] These covalent approaches have been utilized for the solubilization of SWNTs in organic or aqueous media as well as their

incorporation into polymer matrices.[3,31] However, this method of solubilization presents some drawbacks as it alters the intrinsic electrical, mechanical and optical properties of SWNTs. Covalent modification utilizes reactive intermediates that react with the sp^2-hybridized carbon atoms of the SWNT sidewall, resulting in sp^3-carbon defects that damage their intrinsic properties.[28] In addition, covalent chemistry on the surface of SWNTs can reduce their lengths into fragments that range from 100 to 300 nm by refluxing in nitric acid.[15,32]

1.2.2. Non-Covalent Functionalization of SWNTs

Non-covalent functionalization utilizes a dispersant that adsorbs onto the SWNT surface, forming a supramolecular complex that does not disrupt the nanotube's extended π-system.[33,34] This method of functionalization is intriguing since it offers the potential of introducing a reactive handle whilst preserving the desirable electronic properties of SWNTs.[3] A variety of dispersants can be employed for non-covalent functionalization of SWNTs including surfactants,[35–37] aromatic small molecules,[38–40] conjugated polymers,[41–43] and biomacromolecules.[10,44–49] In general, the dispersant molecules interact with the tubular surface of SWNTs through van der Waals or π–π stacking to form a supramolecular complex that is controlled by thermodynamics.[3]

One of the first attempts to disperse carbon nanotubes employing a surfactant was achieved by O'Connell and coworkers in 2002.[10] Their dispersion protocol involved vigorous sonication of a mixture of HiPCO SWNTs and the anionic surfactant sodium dodecyl sulfate (SDS) in H_2O. The mechanical separation of SWNT bundles through

sonication was followed by the interaction of the hydrophobic tails of the surfactant molecules with the SWNT wall, as well as the hydrophilic heads, which create a shell around each individual tube. The resultant SWNT-SDS micelles prevented their re-aggregation, generating a stable dispersion in H_2O. In addition to SDS, other surfactants such as sodium dodecylbenezenesulfonate (SDBS), sodium cholate (SCh), and deoxycholate (DOC) were employed in the dispersion of SWNTs (Figure 4), albeit with no selectivity for different species.[50,51]
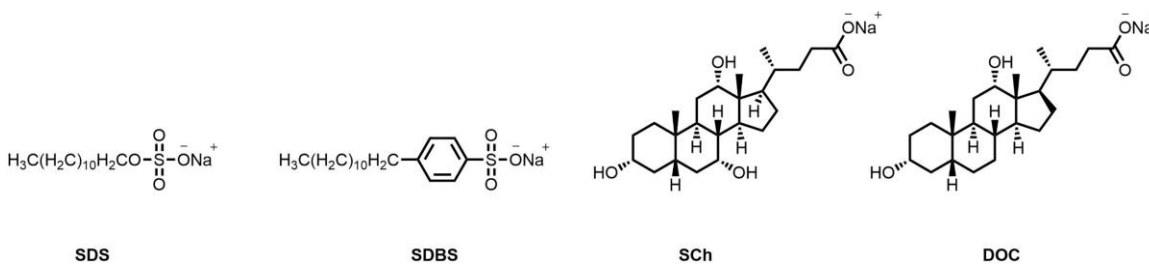
Figure 4. Structures of reported surfactants used in the individualization of SWNTs: sodium dodecyl sulfate (SDS), sodium dodecylbenezenesulfonate (SDBS), sodium cholate (SCh), and deoxycholate (DOC).

Another advancement in the processing of raw nanotubes appeared in 2006, when Arnold et al. reported the aqueous separation of SWNTs using density-gradient ultracentrifugation (DGU).[52] This is a method traditionally used in biochemistry for separating biological macromolecules such as nucleic acids and proteins, based on their buoyant densities.[53] In the study by Arnold *et al.*, surfactant-coated SWNTs in aqueous media were subjected to ultracentrifugation (~200 000 g) in a mass density gradient. In response to the resulting centripetal force, the surfactant-coated SWNTs travel through the density gradient until the density of the medium is identical to their respective buoyant densities.[52] At this point, the aqueous-suspended SWNTs are spatially separated, shown in

Figure 5 as individually coloured bands that contain SWNTs of unique diameter and chirality. The SWNT species can be subsequently extracted employing simple fractionation techniques. Since the introduction of DGU for nanotube purification, numerous studies have been published utilizing this technique,[54–56] in addition to other work which demonstrated that gel electrophoresis allows for separation of nanotubes by electronic type; i.e. semiconducting SWNTs (sc-SWNTs) and metallic SWNTs (m-SWNTs).[57,58]

Despite the progress made with these methods, only sub-microgram quantities of pure SWNT samples can be produced. This is mainly due to the relative inefficiency of these methods, as many iterations of the separation protocol are required for approximately one milligram of a pure SWNT sample. As a result, DGU and gel-based techniques produce costly SWNT samples, making them unsuitable for large-scale, commercial nanotube purification.[13]
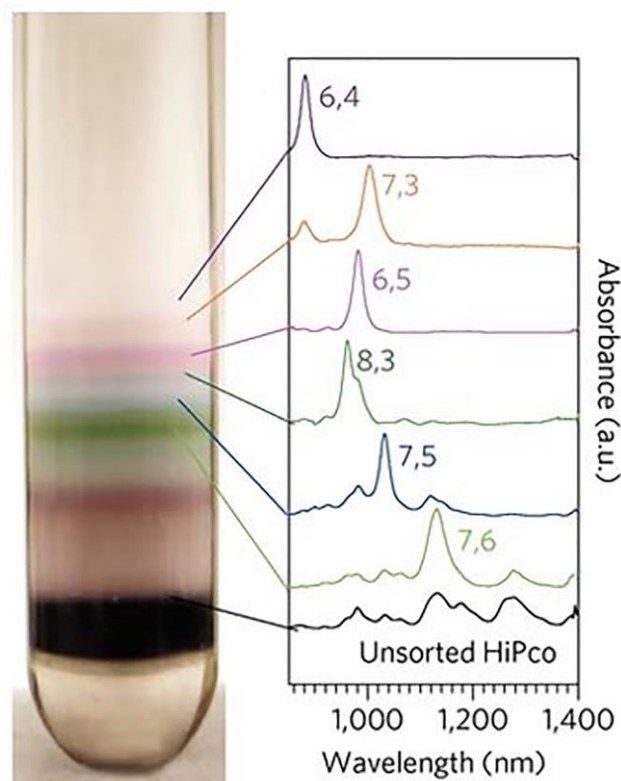
Figure 5. A photograph (left) of a centrifuge tube containing several bands of SWNTs sorted by the density gradient ultracentrifugation (DGU) technique, and their corresponding UV-Vis-NIR absorption spectra (right). Reproduced with permission from [Ghosh, S.; Bachilo, S. M.; Weisman, R. B. *Nat. Nanotechnol.* **2010**, *5* (6), 443–450].[59] Copyright Nature Group, 2009.

DNA is another class of molecules employed in the dispersion of SWNTs. DNA molecules contain nucleotide bases that interact with the surface of SWNTs through π-π stacking interactions, which allows for the DNA strands to helically wrap around SWNTs.[60] In 2009, Zheng and co-workers used highly-specific DNA sequences for the separation and isolation of twelve sc-SWNT chirlaties as shown in Figure 6.[61]
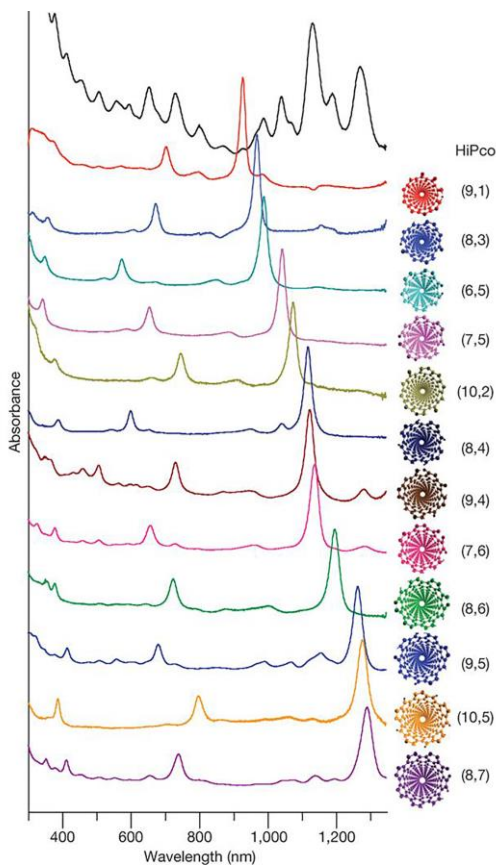
Figure 6. UV-Vis-NIR absorption spectra of 12 sc-SWNT species isolated via DNA and IEX and raw HiPCO SWNTs (top black spectrum). Reproduced with permission from [Tu, X.; Manohar, S.; Jagota, A.; Zheng, M. *Nature* **2009**, *460* (7252), 250–253].[61] Copyright Nature Publishing Group, 2009.

1.2.3. Conjugated Polymers for Non-covalent Functionalization of SWNTs

Compared to the techniques discussed in Section 1.2.2, conjugated polymers are a viable alternative as they offer a scalable and time efficient method for the non-covalent functionalization of SWNTs.[34] Over the past decade, conjugated polymers have been employed for solubilization of carbon nanotubes, and recently have been shown to generate dispersions selective for different SWNT species. Carbon nanotubes are dispersed through

π-stacking interactions between the backbone of the π-conjugated polymer with the SWNT surface. The resultant non-covalent interaction disrupts the intrinsic van der Waals forces in nanotube bundles and prevents their reaggregation.[34] Depending on the flexibility of the polymer backbone, they can either warp helically or simply adsorb onto the nanotube surface to generate polymer-SWNT complexes. This method leads to enhanced dispersions of SWNTs using various conjugated polymers.[62–64] Some of the most studied conjugated polymer structures include polyfluorene, polycarbazole, polythiophene, poly(phenylene vinylene), and poly(phenylene ethynylene)s.[65] Polyfluorenes and their copolymers have been heavily investigated for the electronic separation of SWNTs. They are particularly interesting due to their ease of synthesis and functionalization. Specifically, polyfluorenes have been shown to selectively disperse semiconducting SWNT species.[13] However, there are numerous factors that affect the selectivity in polymer-SWNT interactions such as the polymer backbone and molecular weight, the type of side chains present, as well as the solvents employed for dispersions.[66]

Characterization of SWNTs

Characterization of SWNTs can be achieved through various spectroscopic techniques such as absorbance, photoluminescence (PL), Raman, Rayleigh, and magneto-optical spectroscopy.[67] Absorbance, PL and Raman spectroscopy have become particularly attractive for characterization of SWNTs because they involve rapid, facile sample preparation and cause minimal damage to nanotube samples.[67] The various photophysical processes involved in each spectroscopic method can be described by the electronic density

of states (DOS) diagram of a SWNT, as shown in Figure 7. The absorption process occurs when an incident photon that matches the corresponding excitonic energy difference (E_{ii}), generates an exciton (photoexcited electron and a hole), which is represented by the upward arrow in Figure 7a. The way in which the exciton recombines results in other photophysical processes including Rayleigh scattering, photoluminescence, and Stokes Raman.[67] As shown in Figure 7b, Rayleigh scattering is an elastic process which occurs upon emission of light without the exciton gaining or losing energy. Photoluminescence (Figure 7c) results from excitonic relaxion to the lowest lying excited state (c_1), followed by recombination to emit a lower energy photon (E_{11}), compared to the incident photon. In addition, the exciton may lose or gain energy *via* emission or absorption of a phonon in the scattering process to an intermediate state, resulting in recombination and emission of a scattered photon with slightly lower (E_{22}-E_{ph}) or higher (E_{22}+E_{ph}) energy than the incident photon. These processes are inelastic and are referred to as Stokes (Figure 7d) and Anti-Stokes Raman, respectively.[67]
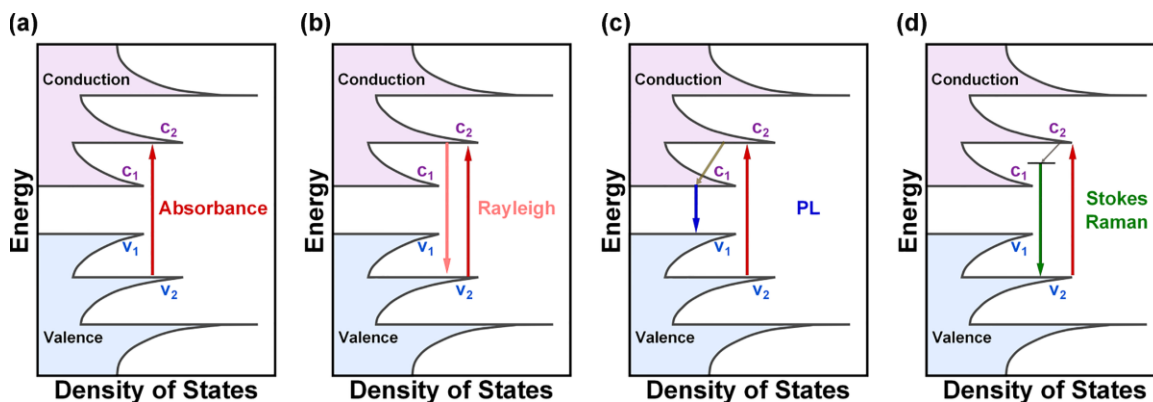
Figure 7. Schematic representation of the various optical processes of SWNTs, such as (a) absorbance, (b) Rayleigh scattering, (c) photoluminescence (PL), and (d) Stokes Raman processes. Reproduced with permission from [Rice, N. A. Separation of Single-Walled Carbon Nanotubes By Electronic Type Using Conjugated Polymers, McMaster University, 2015].[13] Copyright 2015.

1.2.4. Absorption spectroscopy

Absorption spectroscopy is a fundamental, experimentally facile optical measurement for characterization of SWNTs. If the optical features of a nanotube sample are well defined, absorption spectroscopy can provide information on the (*n, m*) chirality distribution of a SWNT sample,[68] as well as the ability of a separation protocol to achieve electronic purity. In 1999, Kataura *et al.* obtained one of the first absorption spectra of SWNTs in thin film samples that were prepared from a dispersion of SWNTs in ethanol.[12] Within the measured spectral range (200 to 2500 nm), only three broad absorbance bands were observed, with no fine features present in the spectrum. Later, in 2002, O'Connell and coworkers obtained an absorption spectrum of SWNTs dispersed with sodium dodecyl sulfate (SDS) in H_2O, where they observed fine features corresponding to various SWNT species present in the sample.[69] Their dispersion protocol involved vigorous sonication of the SDS and SWNTs mixture to detach nanotubes from a bundle and allow for the SDS to

coat nanotubes in order to prevent reaggregation. This was followed by a centrifugation step, which removes any bundles remaining in solution.[70] The individualization of SWNTs in aqueous micellar suspensions resulted in an optical absorption spectrum that contains numerous sharp peaks corresponding to various optical transitions of sc-SWNTs and m-SWNTs in solution. The absorption features of carbon nanotubes arise from the electronic transitions from the valence to conduction bands of the van Hove singularities, where the observed absorption features depend on nanotube diameter and chirality.[70,71] For small diameter HiPCO (0.7 to 1.2 nm) SWNTs, the absorbance features arising from metallic SWNTs is found at approximately 440 to 650 nm (M_{11}) while the semiconducting region is located roughly between 570 to 850 nm (S_{22}) and 850 to 1600 nm (S_{11}).[70,71]

It is therefore possible to assess the electronic nature of a SWNT dispersion considering that the metallic and semiconducting absorptions occur at different regions within the UV-Vis-NIR spectral range. In addition, semi-quantitative information can be collected using absorption spectroscopy by integration of the area under the peaks of metallic and semiconducting regions. However, it is difficult to precisely determine boundaries for integration areas due to the overlap between several spectral excitation regions. Also, the overlap of transitions from numerous SWNT species results in uncertainty when making specific (*n, m*) assignments of a heterogenous sample.[72] Other techniques, such photoluminescence (PL) mapping and Raman spectroscopy are therefore required to obtain a thorough understanding of the sample properties.

1.2.5. Photoluminescence (PL) Mapping

Photoluminescence (PL) Mapping is a spectroscopic technique used to characterize sc-SWNTs, which possess a bandgap and therefore are capable of fluorescence. It measures the fluorescence intensity of sc-SWNTs with respect to multiple excitation and emission wavelengths.[13] PL mapping is a powerful tool for investigation of SWNT dispersions because it offers sensitive qualitative information regarding the presence of specific semiconducting nanotube species. However, the SWNTs in solution must be effectively debundled with limited presence of metallic SWNT species, as such factors can dramatically reduce the observed PL intensity.[73]

The 2D PL map of individualized SWNTs contains numerous peak maxima that can be assigned (*n, m*) values, using data published in the literature.[74] Utilising a tight-binding approximation, it is possible to relate chirality assignments to transition energies and diameters of carbon nanotubes.[75] However, it is difficult to obtain a direct comparison between theoretical and experimental results due to the complexity of the real nanotube as opposed to the suggested approximation. This complexity arises from extrinsic environmental factors such as the presence of other nanotubes, solvents, as well as dispersants, and typically results in a red-shift in the experimentally obtained emission maxima, in addition to broadening of optical features.[76] Nevertheless, it is possible to assign (*n, m*) values for a given SWNT sample by choosing literature data that was acquired under identical or similar environmental conditions as the sample being investigated.

1.2.6. Resonant Raman Spectroscopy

Raman spectroscopy measures the scattered photon intensity with respect to the Raman shift, which is described as the frequency difference (cm^{-1}) between the incident and the scattered photon.[67] It is a versatile and non-destructive technique utilized in probing various sp^2-hybridized carbonaceous materials including metallic and semiconducting SWNTs. In particular, Raman spectroscopy is useful in determining the (*n, m*) distributions[77] as well as characterizing the electronic purity and defect density for both m-SWNTs and sc-SWNTs.[78] In resonance Raman spectroscopy, the incident or scattered photon is at a frequency near the frequency of an electronic transition between the valence and conduction bands of the SWNT. This provides enough energy to excite the electrons to a higher electronic state, resulting in a very large Raman signal. Therefore, resonant Raman spectroscopy offers enhanced signals which allows for detection of SWNTs on a single nanotube level.[79] Figure 8 depicts a plot of electronic transition energies as a function of nanotube diameter and type, generally referred to as a Kataura plot. The horizontal lines depict the excitation wavelengths typically used to study carbon nanotubes, where different excitation wavelengths are in resonance with different SWNT types. This plot shows that multiple excitation wavelengths are required in order to probe the majority of nanotube species within a sample.
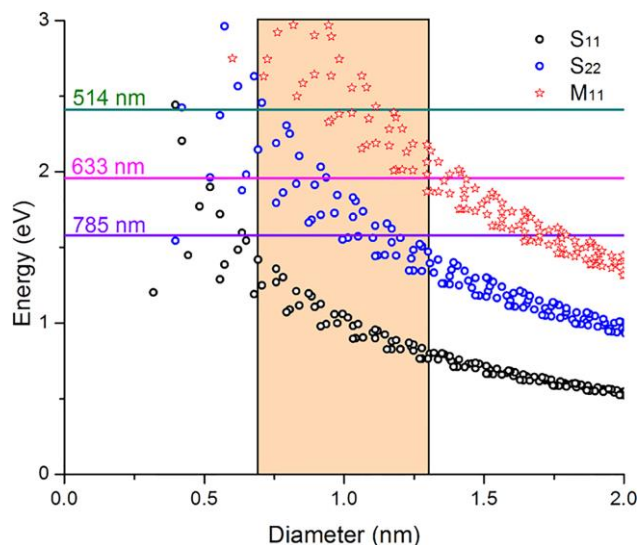
Figure 8. Semiempirical Kataura plot of S_{11} (black), S_{22} (blue) and M_{11} (red). The electronic transitions data for sc-SWNT[74] and m-SWNT[80,81] were obtained from literature sources. The orange box depicts the expected diameter range for HiPCO SWNTs (diameter range from ∼ 0.7 to 1.3 nm). The horizontal lines denote the three laser excitation wavelengths (514, 633, and 785 nm) used for Raman studies in this thesis. Reproduced with permission from [Rice, N. A. Separation of Single-Walled Carbon Nanotubes By Electronic Type Using Conjugated Polymers, McMaster University, 2015].[13] Copyright 2015.

One of the first accounts of resonant Raman experiments on carbon nanotubes was reported by Rao and co-workers in 1997.[82] These experiments were conducted on SWNT powders prepared by laser ablation, and revealed four prominent peaks in the Raman spectrum.[82] Figure 9 shows a typical Raman spectrum for HiPCO SWNTs with the four observed regions, which were later identified as follows: the radial breathing mode (RBM) from ~100 to 400 cm^{-1}, the D-band from ~1250 to 1450 cm^{-1}, the G-band from ~1550 to1595 cm^{-1}, and the G'(or D*) mode at ~2500 to 2900 cm^{-1}.[83]
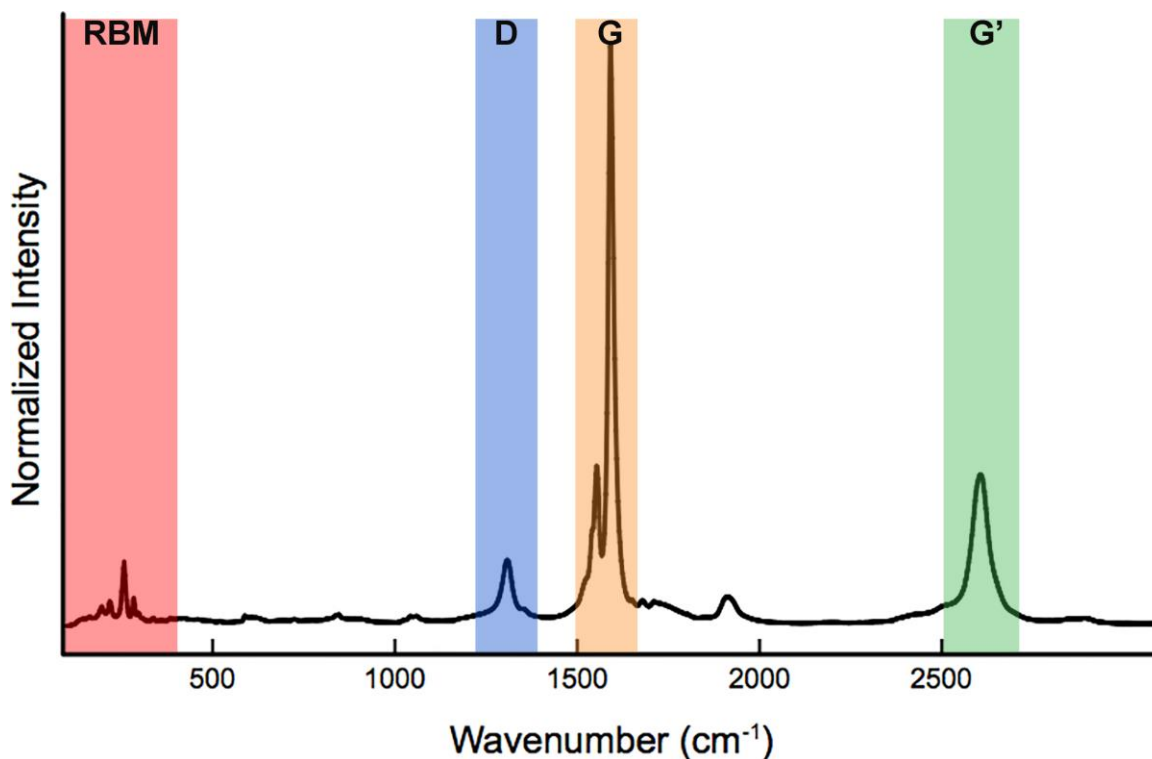
Figure 9. A typical Raman spectrum for a SWNT sample, showing the RBM (red), D-band (blue), the G-band (orange), and G'-band (green) regions.

The four regions shown in Figure 9 provide useful information for the characterization of SWNTs. The RBM region results from the out-of-plane bond stretching of all the carbon atoms in the radial direction, making the RBM mode unique to carbon nanotubes.[83] Thus, the observation of the RBM region in the Raman spectrum is indicative of the presence of SWNTs in a sample.

The D-band, also known as the disorder mode, is found in the Raman spectra of various carbonaceous materials. The disorder mode arises from elastic scattering of electrons by structural defects including vacancies, impurities, or sp^3-hybridized carbon atoms. Thus, the D-band feature is utilized in the determination of the chemical purity of the carbon nanotubes.[84,85]

The G-band mode (also known as the tangential mode) is a Raman feature present in graphitic structures containing sp^2-hybridized carbon atoms, including carbon nanotubes. It results from the in-plane carbon-carbon bond stretches in graphitic materials. The G-band consists of two peaks: A lower frequency G^- and a higher frequency G^+. For sc-SWNTs, both the G^- and G^+ have Lorentzian line shapes, while for m-SWNTs the G^- exhibits a broader Breit–Wigner–Fano (BWF) line shape.[86] Depending on the shape of the G^- mode, it is possible to distinguish between m-SWNTs and sc-SWNTs in a given sample. Raman spectra lacking the BWF line shape in the G-band indicate an absence of metallic SWNTs in the sample. The G'-band (or D*) is a disorder based overtone of the D-mode that is not unique to SWNTs and is found in the Raman spectra of other carbonaceous materials.[83]

1.3. Introduction to Supramolecular Chemistry

The emerging field of modern supramolecular chemistry continues to grow from its humble origins in the early 1960's with the pioneering contributions of Lehn, Cram and Pedersen that were subsequently awarded the Nobel prize in 1987.[87–89] In his Nobel Prize lecture, Lehn describes supramolecular chemistry as "chemistry beyond the molecule,"[87] occurring when two or more chemical species associate through intermolecular forces such as electrostatic interactions, hydrogen bonding, π–π interactions, or van der Waals interactions.[87]

Supramolecular Chemistry is the study of a system composed of molecules or ions which are held together by non-covalent interactions.[90] This field of study may be divided into two distinct categories: i) host-guest chemistry and ii) molecular self-assembly. Host-

guest chemistry involves the non-covalent interactions of a larger (host) molecule enclosing a smaller (guest) molecule to form a supramolecular complex. Meanwhile, self-assembly occurs due to the spontaneous, yet reversible association of two species to form a larger supramolecular complex.[90]

1.3.1. Host-Guest Chemistry

Host-guest chemistry, which is a branch of supramolecular chemistry, explores molecular recognition that enables a guest molecule to bind to the cavity of a host to produce a "host-guest" complex. The host is typically a large molecule that contains a central hole or cavity, such as a synthetic cyclic compound or an enzyme. On the other hand, the guests can vary from small anions and cations, to larger molecules such as linear alkanes or complex hormones.[90] Various host structures have been investigated, including cyclodextrins,[91–93] calixarenes,[94–96] cucurbiturils,[97–99] and pillararenes.[100–102]

1.3.2. Introduction to Pillar[5]arenes

Pillar[5]arenes are macrocyclic molecules belonging to the family of paracyclophanes. Owing to the seminal work by Ogoshi and co-workers,[103] the host-guest chemistry of pillar[5]arenes has attracted significant attention, primarily due to their simple one-step synthesis. Pillar[5]arenes are a class of macrocycles composed of hydroquinone units connected by methylene bridges at the *para*-positions, forming a "pillar-like" structure. The electron-rich dialkoxybenzene moieties of pillar[5]arenes form stable inclusion complexes with various electron-poor molecules, including viologens,[104–106]

alkanediamines,[107,108] and alkylnitriles.[109–111] Host-guest interactions with pillar[5]arenes have been used in polymers,[112–114] sensors,[108,115,116] and organogels.[104,117,118]

1.3.3. First Appearance of Paracyclophanes

The first reported synthesis of paracyclophanes was described by Gribble and Nutaitis in 1985.[119] The synthesis was discovered in an attempt to selectively reduce 4-(hydroxymethyl)diphenyl methanol in the presence of sodium borohydride ($NaBH_4$) and trifluoroacetic acid (TFA), as shown in Scheme 2. Rather than the expected product, 4-(hydroxymethyl)diphenylmethane, two other compounds were observed. Utilising ^{1}H-NMR spectroscopy and mass spectrometry, it was apparent that the mixture of products was composed of the novel paracyclophanes **1** and **3**. It was hypothesized that these novel paracyclophanes resulted from a Friedel-Crafts cyclo-oligomerization of the initially formed **5**. It was later confirmed that TFA promoted the Friedel-Crafts alkylation of arenes with benzyl (or related) alcohols.[119]
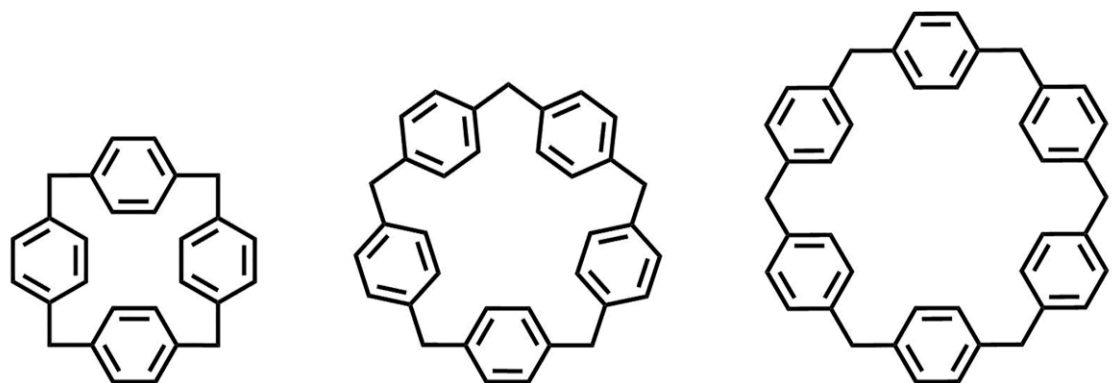
Scheme 1. Structures of various paracyclophanes.
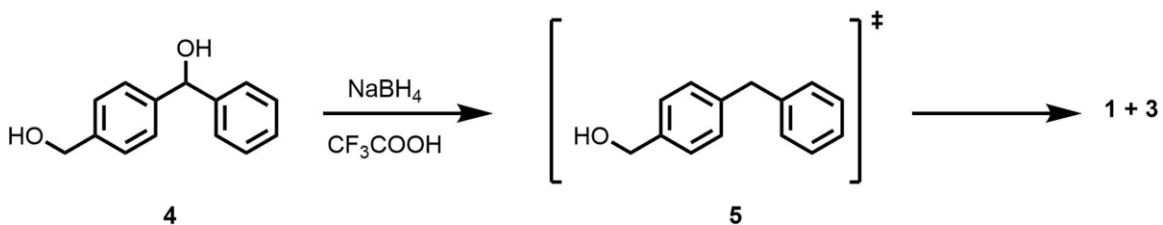
Scheme 2. The macrocycles obtained during the selective reduction of **4**.

Given the findings of their reaction, Gribble and Nutaitis sought to further investigate the Friedel-Crafts cyclo-oligomerization of various benzyl alcohol derivatives. As shown in Scheme 3, they began with commercially available 4-bromobenzophenone (**6**) to obtain the precursors **7**, **8**, and **9** utilizing a repetitive three-step homologation method. The conversion of alcohols **7**, **8** and **9** to their corresponding paracyclophanes involved reflux in the presence of TFA. While this resulted in low yields of **2** and **3**, the formation of the cyclotetramer **1** was not observed. Regardless of further optimization, the macrocyclization step still generated low yields of **2** and **3**.
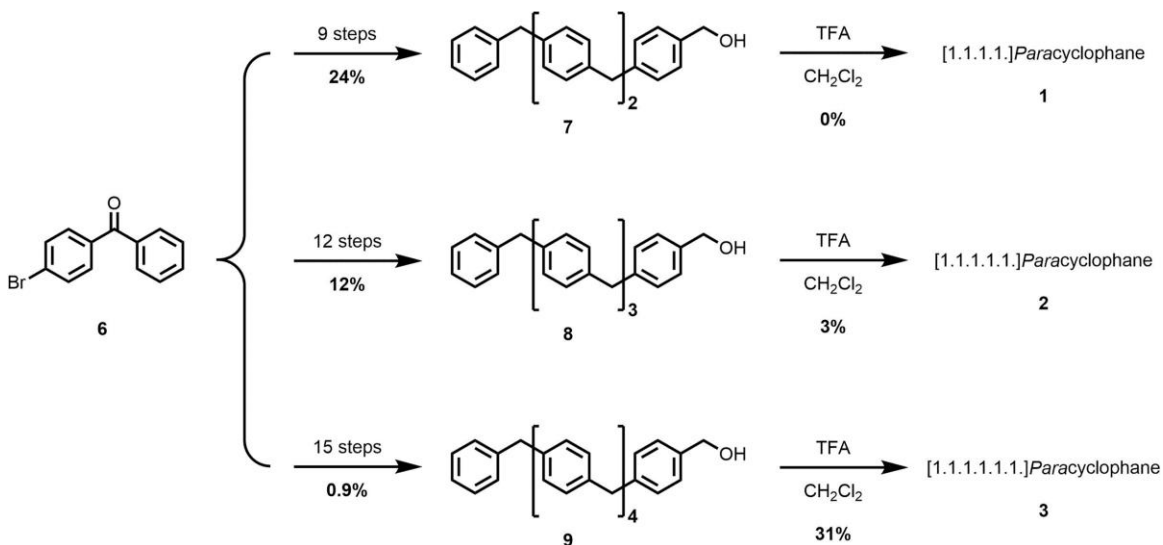
Scheme 3. Multi-step synthesis of paracyclophanes **1**, **2**, and **3**.

Despite the fact that the chemistry of other cavitands, such as calixarenes, was popular due to their one-step, high-yielding synthesis and their ease of functionalization,[120–122] the chemistry of pararcyclophanes did not receive much attention due to their multi-step, low yielding synthesis.

1.3.4. First Efficient Synthesis of Pillar[n]arenes

In 2008, Tomoki Ogoshi published an efficient synthesis for hydroquinolic derivatives connected by methylene bridges at the *para* positions (Scheme 4).[103] Owing to their pillar-like structure, Ogoshi named these macrocyclic structures "pillar[n]arenes", where *n* corresponds to the number of aromatic repeat units. The efficient, one-step synthesis of the cyclopentamer (*n* = 5) involved the reaction of commercially available 1,4-dimethoxybenzene with paraformaldehyde in the presence of a Lewis acid catalyst in dichloromethane and 1,2-dichloroethane. Under these reaction conditions, they obtained

exclusively pillar[5]arene in 22% yield.[103] The yield was improved to 71% upon reaction of one equivalent of the 1,4-dimethoxybenzene with three equivalents of paraformaldehyde. As a result of their facile and high-yielding synthesis from commercially available starting materials, the chemistry of pillar[5]arenes received significant attention within the scientific community.
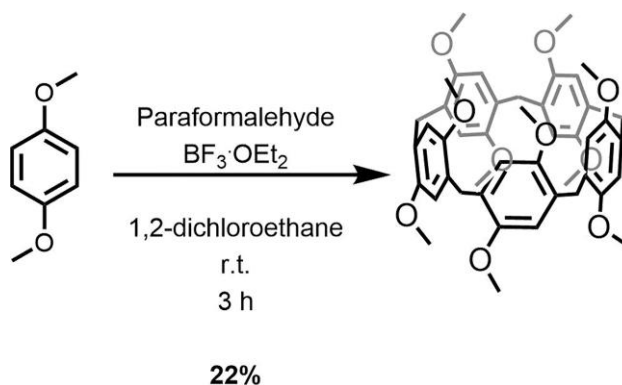
Scheme 4. First efficient synthesis of pillar[5]arene reported by Ogoshi in 2008.

1.3.5. Synthesis of Pillar[5]arenes under Thermodynamic Control

The formation of a macrocycle is a generally low-yielding reaction where formation of linear oligomers and polymers generally predominates.[123,124] As a result, high-dilution techniques are employed to facilitate cyclization, hence increasing the overall yield of macrocycle formation.[124] In 2011, Nierengarten and co-workers reported that the high-yielding synthesis of pillar[5]arenes occurs under thermodynamic control.[125] They found that the cyclo-oligomerization between 2,5-bis(bromomethyl)-1,4-dialkoxybenzene and 1,4-dialkoxybenzene did not generate the expected cyclohexamer. Rather, they observed solely the formation of pillar[5]arene. Thermodynamic control is possible due to the reversibility of the Friedel Crafts reaction. As the formation of the cyclization products is

carried out under thermodynamic control, their distribution depends on the relative stabilities of the final products (Figure 10). Nierengarten and co-workers concluded that the pillar[5]arene derivative is the thermodynamic product. They reported X-ray diffraction data for the product, which showed that the 1,4-dimethoxypillar[5]arene methylene bridge bond angle is 111.3°. This value is in accordance with the bond angle of sp^3-hybridized carbons (109.5°) and the theoretical internal bond angle (108°) for a regular, unstrained pentagon.[126]
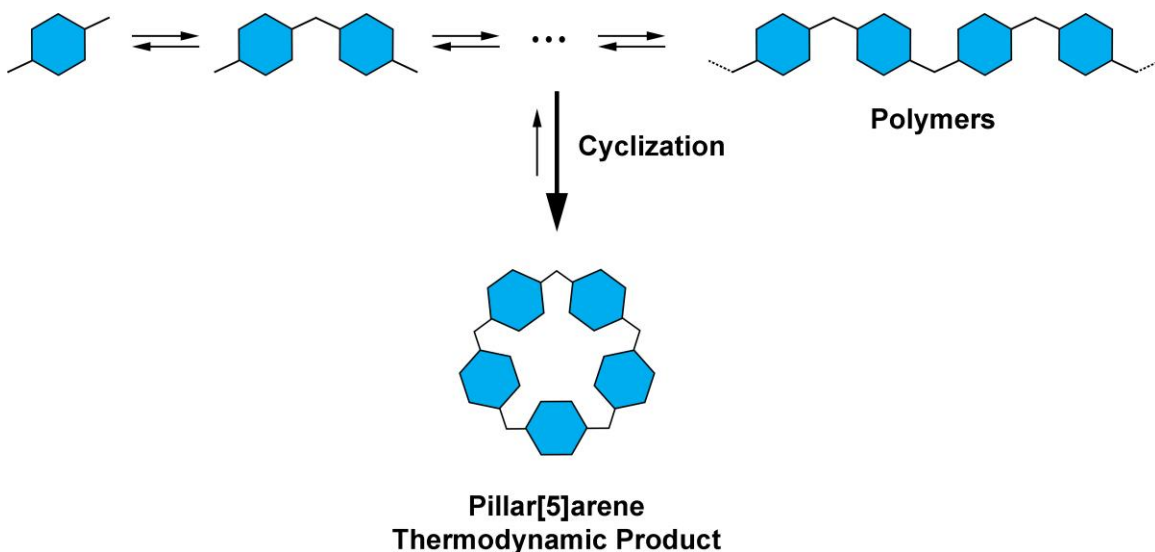
Figure 10. Schematic representation for the proposed pathway of pillar[5]arene under thermodynamic control.

1.3.6. Mono-functionalization of Pillar[5]arenes

In order to introduce additional functionality to pillar[5]arenes, they must be made reactive *via* incorporation of side chains containing alkyl bromide, alkyl azide, or alcohol moieties. Scheme 5 shows two reported approaches for the mono-functionalization of pillar[5]arenes that do not alter their host-guest properties.[127] The first method involves the

co-cyclization of two distinct monomers where one contains the desired reactive handle. In 2011, Stoddart and co-workers demonstrated that it is possible to prepare a co-pillar[5]arene by reaction of 1,4-dimethoxybenzene and 1-(2-bromoethoxy)-4-methoxybenzene in the presence of paraformaldehyde and $BF_3 \cdot OEt_2$.[108] The resultant mono-azide pillar[5]arene can undergo copper-mediated azide-alkyne cycloaddition (CuAAC) with a terminal alkyne to prepare a pillar[5]arene derivative.[108,128–130]

The second strategy for mono-functionalization of pillar[5]arenes was employed by Ogoshi and co-workers in 2011.[131] They achieved the mono-demethylation of dimethoxy pillar[5]arene using less than one equivalent of BBr_3 and isolated the product in 22% yield. The reaction was later optimized by Cao and coworkers, utilising four equivalents of BBr_3 with freshly distilled chloroform, and stirred at -5 °C to obtain a 60% yield of the mono-functionalized pillar[5]arene.[131] The pillar[5]arene bearing a single hydroxyl group, can be further functionalized under Williamson ether synthesis conditions to generate novel pillar[5]arene derivatives.[132,133]

Approach 1: Co-cyclization
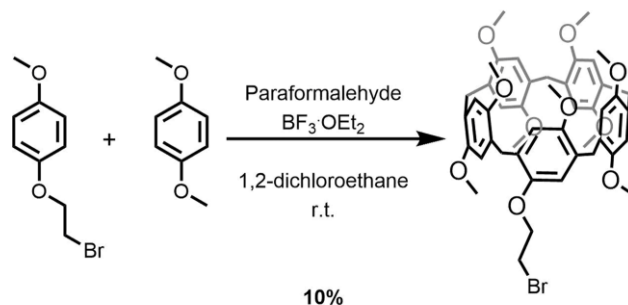
Approach 2: Deprotection
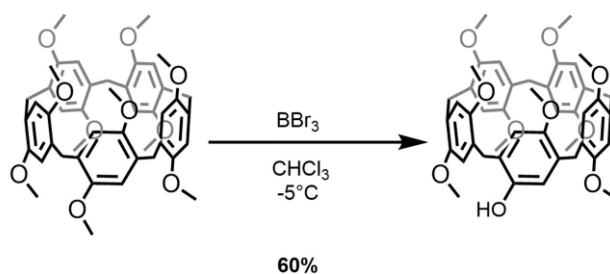
Scheme 5. Two approaches for the mono-functionalization of pillar[5]arenes.

1.3.7. Host-guest Properties of Pillar[5]arenes

Pillar[5]arenes are host molecules with symmetrical central cavities that are approximately 5 Å in diameter.[134] The inner cavity of pillar[5]arene is electron rich due to the electron-donating alkoxy moieties located at the rim. In addition, the pillar-like structure enhances their π-electron density, making pillar[5]arenes excellent hosts for guests containing cationic or electron-withdrawing groups.[134] There are several reports within the literature demonstrating that pillar[5]arenes form inclusion complexes with aromatic compounds like pyridinium and viologen derivatives,[105,135] as well as linear

alkanes containing electron-withdrawing amine,[136] ammonium,[136] cyano,[137] and halogen[138] end groups.

Supramolecular titration is a common method utilized in quantitative analysis of the intermolecular interactions between a host (such as pillar[5]arenes) and a guest molecule. It involves gradual addition of one component (typically the guest) to the system (host) while monitoring a physical property such as a specific chemical resonance (NMR spectroscopy) or absorption band (UV-Vis spectroscopy) that is sensitive to the supramolecular interaction(s) of interest.[139] The acquired spectroscopic data is then compared and fitted to a binding model to obtain information about the system, such as the association constant (K_a).[139] Host-guest interactions formed with pillar[5]arenes have found applications in materials such as polymers,[112–114] sensors,[108,115,116] and organogels.[104,117,118]

1.4. Objectives

To date, most structural modifications have aimed to achieve enriched dispersions of semiconducting SWNTs, with recent efforts aimed toward developing polymer backbone structures capable of conformational changes or depolymerization in response to a stimulus.[140–144]

Recently, we have prepared polyfluorene derivatives possessing azide groups in their side chains, and then used these derivatives to noncovalently functionalize SWNTs.[145–147] We have demonstrated that it is possible to decorate the resulting polymer-SWNT complex using the Strain-Promoted Azide-Alkyne Cycloaddition (SPAAC)[147] or

the Copper-Mediated Azide-Alkyne Cycloaddition (CuAAC).[146] These results indicate that conjugated polymer side chains can be tuned to impart interesting characteristics to the polymer-SWNT complex. The aim of this project is to utilize the same design principle to produce polymer-SWNT complexes that contain macrocycles in the polymer side chains to influence the dispersion properties of the resulting polymer-SWNT complex.

Macrocycles have received intense interest in the literature,[148–153] and encompass several key scaffolds that include cyclodextrins,[91–93] calixarenes,[95,96,154] cucurbiturils,[97–99] and pillararenes.[100,155,156] Owing to the seminal work by Ogoshi and co-workers,[103] pillar[5]arenes have attracted significant attention due to their facile one-step synthesis and their unique structure, composed of hydroquinone units connected by methylene bridges at the *para*-positions that form a "pillar-like" structure. These pillar[5]arenes can be further derivatized to install a single functional handle that can be used in subsequent functionalization. The electron-rich dialkoxybenzene moieties of pillar[5]arenes form stable inclusion complexes with various electron-poor molecules, including viologens,[104–106] alkanediamines,[107,108] and alkylnitriles.[109–111] Host-guest interactions with pillar[5]arenes have been used in polymers,[112–114] sensors,[108,115,116] and organogels.[104,117,157] The aim of this study is to explore the incorporation of pillar[5]arenes onto the surface of a polymer-SWNT complex. The first main objective is to characterize the dispersion properties before and after macrocycle incorporation using UV-Vis-NIR, Raman, and fluorescence spectroscopy, and determine the SWNT concentration in solution using thermogravimetric analysis (TGA). The second objective is to incorporate the cavitand-containing polymer-SWNT dispersion into an organogel using a bis(alkylnitrile)-

functionalized polymer as a crosslinking agent. The final goal of this project involves characterization of the organogel before and after incorporation of SWNTs by determining their Young's Modulus.

Chapter 2: Preparation and Characterization of Polymer-SWNT Complexes

2.1. Introduction

Chapter 2 focuses on the synthesis and functionalization of polyfluorene to generate a pillar[5]arene-functionalized conjugated polymer. The synthetic approach involved preparation of a polyfluorene that contains alkyl bromides in the side chain that can be coupled with a mono-hydroxylated pillar[5]arene in the presence of a base and a phase transfer catalyst. The alkyl bromides of the polyfluorene serve as reactive handles for further functionalization of the polymer, such that the nucleophilic pillar[5]arene derivative attacks the electrophilic carbon of the alkyl bromide side chains to generate the macrocycle-functionalized polymer. Also, the preparation and characterization of the polymer-SWNT dispersions are discussed in this chapter. In addition, the host-guest properties of the polymer-SWNT dispersion are explored using ^{1}H-NMR spectroscopy.

2.2. Polymer Synthesis

To prepare the macrocycle-containing polymer-SWNT complex, we first synthesized a polyfluorene derivative containing alkyl bromides (**PF-Br**) according to literature procedures (see Appendix B: Synthetic Procedures for details).[158] GPC analysis of **PF-Br** revealed that the polymer had a number average molecular weight (M_n) of 31 kDa and a dispersity (Đ) of 2.02. Separately, the ethoxy derivative of pillar[5]arene was prepared *via* condensation of 1,4-diethoxybenzene with paraformaldehyde in the presence of $BF_3 \cdot OEt_2$ (Scheme S3). The resulting structure was then mono-de-ethylated using BBr_3,

resulting in the mono-hydroxylated pillar[5]arene **6**. This moiety was introduced into the conjugated polymer scaffold by coupling **PF-Br** with **6** *via* phase transfer alkylation, to afford the pillar[5]arene-containing polyfluorene, **PF-Pillar** (Scheme 6). As shown in Figure 11, the ^{1}H NMR signal at 3.30 ppm in **PF-Br**, which corresponds to the methylene group adjacent to the alkyl bromide, shifts to 3.76 ppm in **PF-Pillar**. This downfield shift of the resonance upon alkylation is indicative of the quantitative conversion from the alkyl bromide to the alkyl ether product.
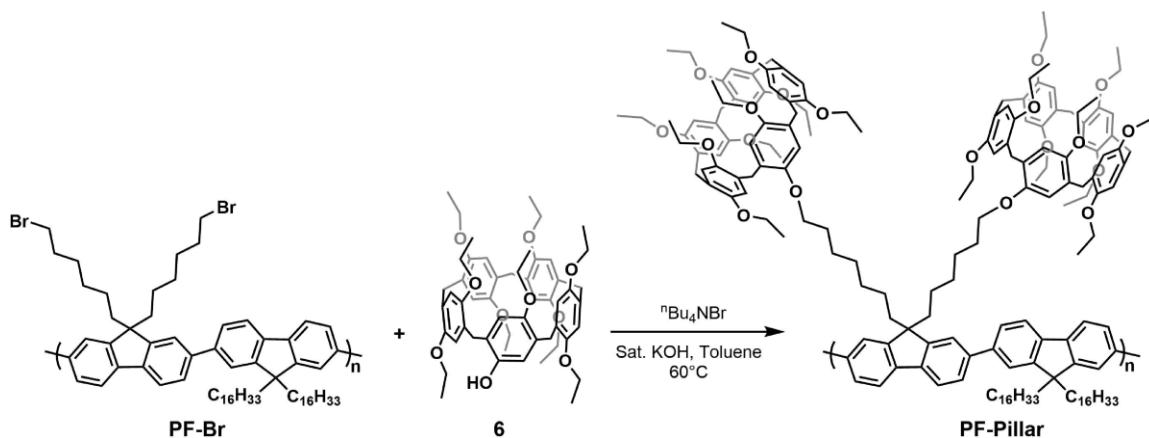
Scheme 6. Post-polymerization functionalization of **PF-Br** with **6** to afford **PF-Pillar**.
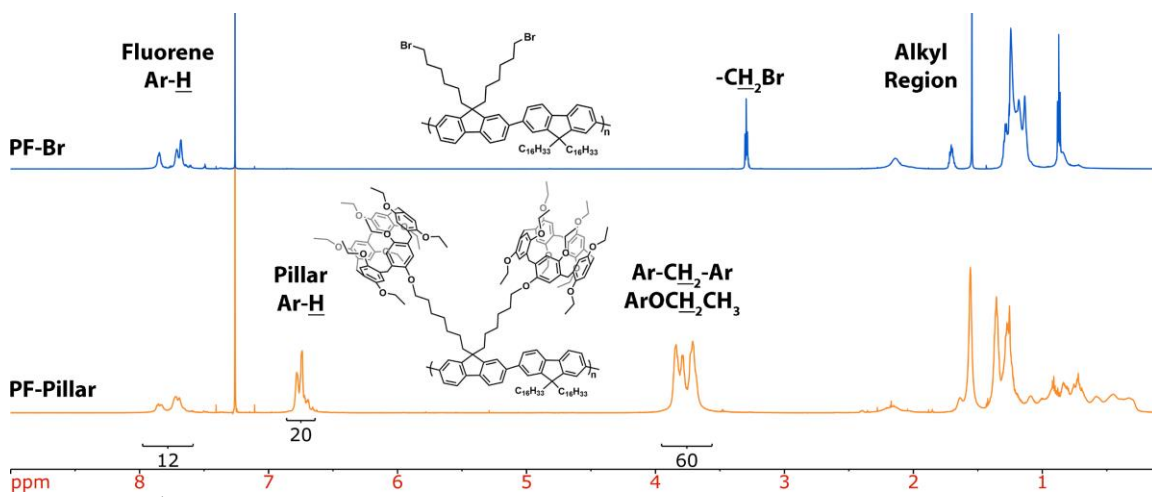
Figure 11. ^{1}H-NMR spectra overlay of **PF-Br** (blue) and **PF-Pillar** (orange) in CDCl₃.

2.3.   Preparation of Polymer-SWNT Dispersions

With our polymers in hand, polymer-SWNT dispersions were prepared with raw HiPCO SWNTs following modified literature procedures.[159] As shown in Figure 12, HiPCO SWNTs (5 mg) were added to a solution of polymer (10 mg of **PF-Br** or **PF-Pillar**) in THF (10 mL). The mixture was then sonicated for 2 h in a bath sonicator chilled with ice. The resultant black suspension was centrifuged at 8,346g for 30 min, and the supernatant was carefully isolated to obtain the polymer-SWNT dispersion, which was stable on the benchtop for at least several months.
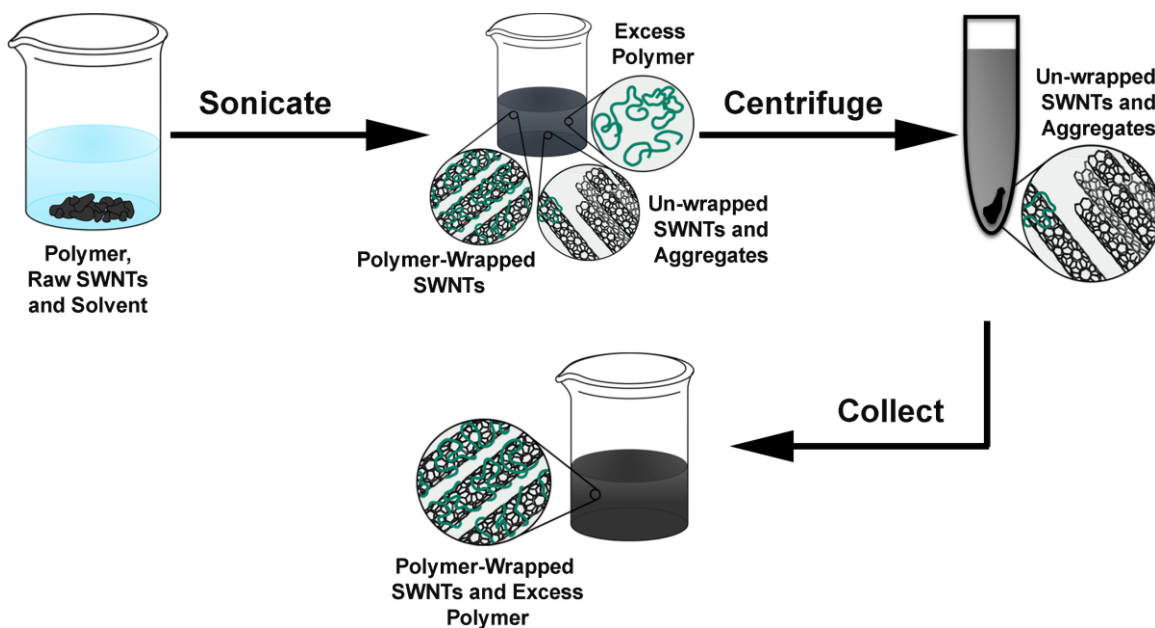
Figure 12. Protocol for preparation of polymer-wrapped-SWNT dispersions in organic solvent.

2.4.   Characterization of the Polymer-SWNT Dispersions

To characterize the polymer-SWNT dispersion, we first performed UV-Vis-NIR spectroscopy. The absorption features within the spectral range can be grouped into three

categories: Two semiconducting regions, S_{11} (830 – 1600 nm) and S_{22} (600 – 800 nm), and a metallic region, M_{11} (440 – 645 nm).[71] As shown in Figure 2, the as-produced **PF-Br**-SWNT dispersion possesses sharp absorption features that reach a maximum intensity of ~0.9. The absence of a broad exponential background suggests at least some degree of sc-SWNT species enrichment. In contrast, the as-produced **PF-Pillar**-SWNT dispersion was highly concentrated and exhibited absorptions in the metallic as well as the semiconducting regions (Figure 13). The as-produced **PF-Pillar**-SWNT dispersion was too concentrated for measurement and required a five-fold dilution to obtain the absorption spectrum shown in Figure 13. We hypothesize that steric bulk imparted by the pillar[5]arene side chains allows for effective steric stabilization of the colloidal polymer-SWNT dispersion.
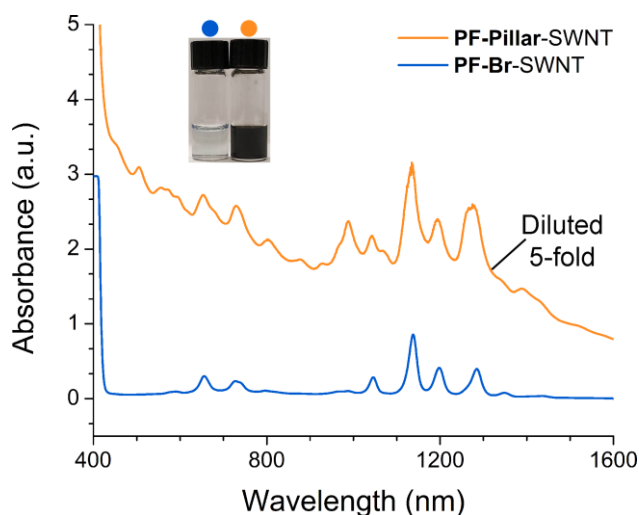
Figure 13. UV-Vis-NIR absorption spectra of polymer-SWNT dispersions (2:1 polymer:SWNT mass ratio) in THF for **PF-Pillar**-SWNT (orange) and **PF-Br**-SWNT (blue). The absorption spectrum for **PF-Pillar**-SWNT was diluted five-fold in THF.

To further probe the polymer-SWNT dispersions, we employed TGA to calculate SWNT concentration. Samples for TGA were prepared by filtering a known aliquot of polymer-SWNT dispersion (0.5 – 6 mL) through a Teflon membrane with 0.2 μm pore

diameter and then washing with THF until the filtrate did not fluoresce at 365 nm. The samples were then transferred to the TGA crucible to determine the recovered mass of polymer-SWNT complex. As shown in Figure S1, samples were heated to 500 °C under an argon atmosphere at a rate of 15 °C·min^{-1}. Polymer-only samples were also recorded under identical experimental conditions, and the mass losses, which correspond to polymer side chain degradation, could be used to calculate the SWNT mass fraction (f_{SWNT}) (see Appendix C for calculations). Given a known volume of polymer-SWNT dispersion ($V_{polymer\text{-}SWNT}$) containing a known mass of polymer-SWNT complex ($m_{polymer\text{-}SWNT}$), the SWNT concentration (c_{SWNT}) could be calculated as:

$$c_{SWNT} = \frac{f_{SWNT} \times m_{polymer-SWNT}}{V_{polymer-SWNT}} \qquad (3)$$

The relevant data are tabulated in Table S1, and c_{SWNT} for the **PF-Br**-SWNT and **PF-Pillar**-SWNT dispersions were determined to be 20 and 600 µg·mL^{-1}, respectively. These results demonstrate that the introduction of macrocyclic structures onto the polymer side chains is effective at producing unusually concentrated SWNT dispersions using small amounts of polymer (~30-fold increase in SWNT concentration using a 2:1 polymer:SWNT mass ratio). In comparison, a number of reports describe polymer:SWNT mass ratios in excess of 50:1, only to produce relatively dilute dispersions.[160,161]

We then performed Raman spectroscopy to investigate the differences in the SWNT populations dispersed by **PF-Br** and **PF-Pillar**. The samples were prepared by drop-casting the dispersions onto a silicon wafer and evaporating the solvent at room temperature. A reference sample containing raw HiPCO SWNTs was prepared by sonicating the raw SWNTs in CHCl$_3$ and then drop-casting the suspension onto a silicon

wafer. Raman scans were obtained using excitation wavelengths at 514, 633, and 785 nm, as it has been shown that these excitation wavelengths are sufficient for the characterization of the electronic properties of HiPCO SWNTs.[162] Figure 14 shows the radial breathing mode (RBM) of the Raman spectra at the three excitation wavelengths (full Raman spectra are provided in Figure S2). The spectra were normalized to the G-band at ~1590 cm^{-1} and offset for clarity. In the RBM region at 514 nm, predominantly m-SWNT features (225 to 290 cm^{-1}) are observed.[163] The **PF-Pillar**-SWNT sample exhibits peaks in this region, while the **PF-Br**-SWNT sample does not (Figure 14a). This suggests that, under identical dispersion preparation conditions, **PF-Pillar** disperses m-SWNTs, while **PF-Br** does not. This result is further corroborated by G-band analysis (inset of Figure 14a). The G-band consists of two peaks: A lower frequency G$^-$ and a higher frequency G$^+$. For sc-SWNTs, both the G$^-$ and G$^+$ have Lorentzian line shapes, while for m-SWNTs the G$^-$ exhibits a broader Breit–Wigner–Fano (BWF) line shape.[86] A broad G$^-$ band is observed for the **PF-Pillar**-SWNT sample, which is consistent with the presence of m-SWNTs. Meanwhile, the **PF-Br**-SWNT sample lacks the BWF line shape in the G-band, confirming that m-SWNTs are absent. At 633 nm, both m-SWNTs (175−230 cm^{-1}) and sc-SWNTs (230−300 cm^{-1}) are in resonance.[86,164] As shown in Figure 14b, the **PF-Pillar**-SWNT sample exhibits peaks corresponding to both sc- and m-SWNTs. However, only sc-SWNTs peaks are present in the **PF-Br**-SWNT sample. Lastly, at 785 nm sc-SWNTs are primarily in resonance.[163,165] A few large diameter metallic species, most notably the (16,7) and (12,9) species, are also observed in the low-frequency region. Figure 14c shows that sc-SWNTs are present in both the **PF-Br**-SWNT and **PF-Pillar**-SWNT samples. Again, this demonstrates that **PF-Br**

disperses only sc-SWNTs, while **PF-Pillar** disperses both sc- and m-SWNTs. Beyond sc-SWNT peaks at 785 nm, a prominent peak at 265 cm^{-1} arises from the (10,2) sc-SWNT species when trapped in a SWNT bundle. Assuming (10,2) is present, this "bundling peak" can be used to identify the degree of bundling in a nanotube sample.[159] It was found that the bundling peak for both polymer-SWNT samples was substantially supressed compared to the raw SWNT sample. Overall, the Raman data demonstrates that the concentrated **PF-Pillar**-SWNT sample is a function of unusual colloidal stability, rather than due to the suspension of SWNT bundles.
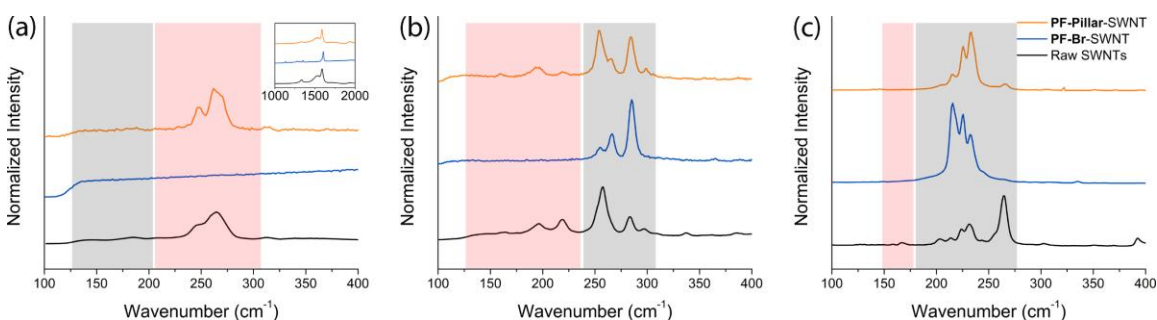
Figure 14. RBM regions at (a) 514, (b) 633, and (c) 785 nm excitation wavelengths. Raman spectra The gray boxes denote the signals arising from sc-SWNTs, while the pink boxes indicate the locations of signals from m-SWNTs. The inset in (a) shows the G-band region, located at ~1590 cm^{-1}, upon excitation at 514 nm.

To further characterize the polymer-SWNT dispersions, photoluminescence (PL) maps were obtained. The polymer-SWNT dispersions were diluted in THF to obtain an absorption intensity of ~0.11 for the peak centred at ~1279 nm (Figure S3). The excitation and emission energies of various sc-SWNTs were obtained from experimental Kataura plots and plotted on the PL map.[74] As shown in Figure 15a, high intensity PL signals were observed in the **PF-Br**-SWNT dispersion, with the most intense peak corresponding to the (7,6) sc-SWNT species. Other prominent species include (8,7), (8,6), and (7,5). For the **PF-**

Pillar-SWNT dispersion, the (7,6) species is also the most intense species. Other prominent species include (9,4), (7,5), (6,5), and (8,4). Interestingly, the relative fluorescence intensity of the **PF-Pillar**-SWNT sample is roughly two orders of magnitude lower compared to the **PF-Br**-SWNT sample. The reduced fluorescence intensity in **PF-Pillar**-SWNT may be attributed to either SWNT bundles or m-SWNT species present in the sample, as both are known fluorescence quenchers.[11] As Raman analysis indicates the lack of significant bundling in the polymer-SWNT dispersions, we attribute the observed fluorescence quenching to an increased amount of m-SWNTs dispersed by **PF-Pillar**, which is consistent with the aforementioned analyses.
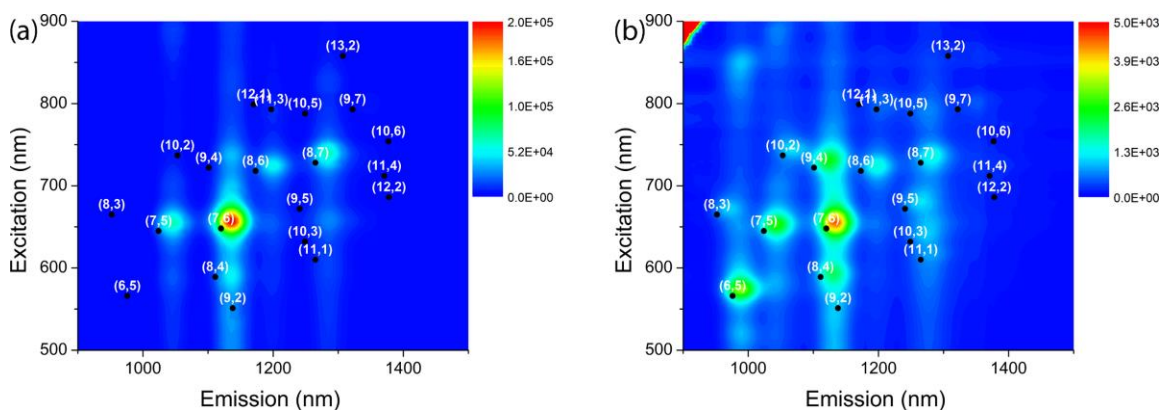
Figure 15. Photoluminescence maps of (a) **PF-Br**-SWNT and (b) **PF-Pillar**-SWNT, concentration-matched by UV-Vis-NIR and plotted on the same scale.

2.5. Host-Guest Properties of Polymer-SWNT Dispersion

With our polymer-SWNT dispersions fully characterized, we sought to explore the dispersion properties of the **PF-Pillar**-SWNT sample using ^{1}H-NMR spectroscopy. We employed ^{1}H-NMR to investigate the host-guest interactions in the presence of our polymer-SWNT sample. We first examined the host-guest interactions between **PF-Pillar** and 1,6-dicyanohexane in THF-d_8 (Figure S4). The resonance at 6.84 ppm, which

corresponds to the aromatic protons in pillar[5]arene, was shifted downfield by 0.07 ppm upon the addition of 1,6-dicyanohexane. This downfield shift is consistent with the association between 1,6-dicyanohexane and a pillar[5]arene-functionalized conjugated polymer.[166] To investigate the properties of the **PF-Pillar**-SWNT complex, we prepared a **PF-Pillar**-SWNT dispersion in THF-d_8 (0.75 mL), following the previously outlined protocol (*vide supra*), and added hexamethyldisilane (0.5 µL) as an internal standard. NMR spectra were normalized to this internal standard (for full ^{1}H-NMR spectra, see Figure S5). Compared to **PF-Pillar**, the ^{1}H-NMR spectrum of the **PF-Pillar**-SWNT dispersion in THF-d_8 shows broad signals which correspond to the fluorene backbone as well as the pillar[5]arene moiety (Figure 16). Upon addition of 1,6-dicyanohexane, the resonance corresponding to the aromatic pillar[5]arene protons shifts from 6.83 ppm to 6.91 ppm, with slight broadening. Thus, it is apparent that the host-guest chemistry between the pillar[5]arene moiety and 1,6-dicyanohexane occurs in the presence of the polymer-SWNT complex.
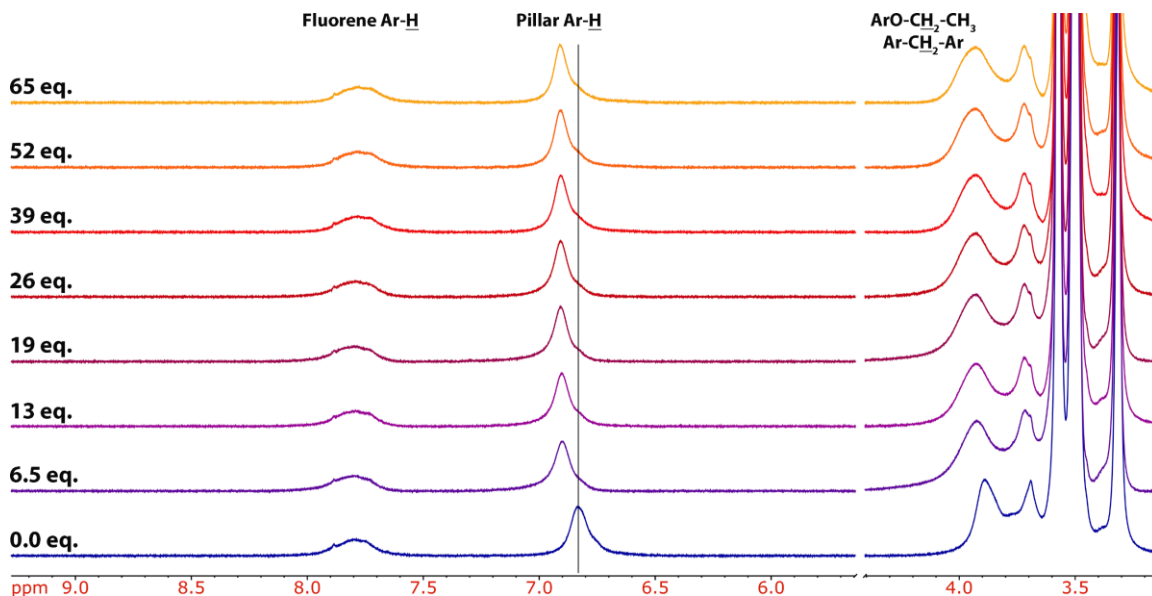
Figure 16. ^{1}H-NMR spectra (THF-d$_8$, 298 K) of the **PF-Pillar**-SWNT dispersion recorded after successive additions of 1,6-dicyanohexane (0 – 65 eq).

2.6. Summary

This chapter explored the synthesis and characterization of a macrocycle-containing conjugated polymer as well as its effect on the solubility of carbon nanotubes. The post-polymerization functionalization of polyfluorene bromide was utilized to prepare a pillar[5]arene-derivatized polyfluorene, as evidenced by ^{1}H-NMR spectroscopy. UV-Vis-NIR spectroscopy and thermogravimetric analysis showed that the non-covalent functionalization of SWNTs with the macrocycle containing polyfluorene significantly enhanced nanotube solubility. This resulted in a dark and concentrated nanotube dispersion, compared to that of the polyfluorene bromide precursor. Also, analysis of the polymer-SWNT dispersions by UV-Vis-NIR, Raman, and Photoluminescence spectroscopy revealed that the initial polyfluorene derivative preferentially dispersed sc-SWNT species, while the pillar[5]arene-decorated polyfluorene produced dispersions

containing both sc-SWNTs and m-SWNTs. The host-guest properties of the pillar[5]arene-decorated polyfluorene SWNT dispersion was investigated using ^{1}H-NMR spectroscopy. It was found that the formation of an inclusion complex between pillar[5]arene and 1,6-dicyanohexane occurred in the presence of the macrocycle-containing polymer-SWNT complex.

Chapter 3: Preparation and Characterization of Supramolecular Organogels

The experiments outlined in Chapter 3 build on the host-guest properties of the macrocycle-containing polymer-SWNT complex. Host-guest interactions formed with pillar[5]arenes have found applications in materials such as polymers,[112–114] sensors,[108,115,116] and organogels.[104,117,118] Recently, we have explored the host-guest interactions of a pillar[5]arene functionalized conjugated polyimine scaffold with various alkylnitrile guests.[166] We prepared self-healing organogels made by the pillar[5]arene-alkylnitrile inclusion complexes. However, the gels were mechanically weak due to the inherently weaker crosslinks between the pillar[5]arene and alkylnitrile polymer chains.[167,168] Organogel stiffness can be improved *via* the introduction of a reinforcer such as carbon nanotubes.[169–171] Considering that carbon nanotubes have a high Young's Modulus (up to 1 TPa) and a high aspect ratio, they may be effective for reinforcement with minimal SWNT loading.[172–175] This chapter explores the incorporation of the pillar[5]arene-containing polymer-SWNT complex into a supramolecular organogel. Chapter 3 focuses on the preparation and characterization of the supramolecular organogels, beginning with the synthesis of a crosslinking polymer containing terminal alkyl nitriles. Then, we explore its interaction with the pillar[5]arene-decorated polyfluorene to generate a supramolecular organogel. Finally, we investigate the difference in mechanical properties of the organogel before and after SWNT incorporation.

3.1. Preparation of Supramolecular Organogels

Having confirmed the formation of inclusion complexes in the presence of the **PF-Pillar**-SWNT dispersion (Chapter 2.5), we sought to incorporate the concentrated dispersion into supramolecular organogels. Initially, we envisioned a crosslinked network of pillar moieties on **PF-Pillar** with a polyfluorene containing alkyl nitrile side chains (**PF-CN**) through combination of equimolar ratios of **PF-Pillar** and **PF-CN**. We expected the pillar[5]arene structures on the **PF-Pillar** to form inclusion complexes with the alkyl nitriles of **PF-CN**, making a "zipper-like" organogel (Figure 17).
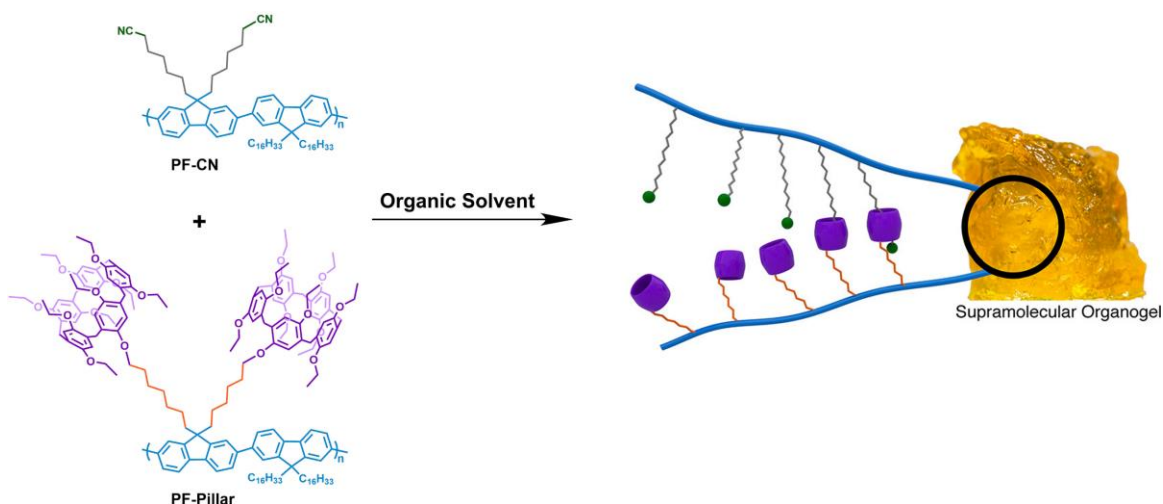
Figure 17. Cartoon representation of host-guest driven gelation of **PF-Pillar** (purple) and **PF-CN** (green). Adapted from [Kardelis, V.; Li, K.; Nierengarten, I.; Holler, M.; Nierengarten, J. F.; Adronov, A. *Macromolecules* **2017**, *50* (23), 9144–9150].[166]

Thus, we attempted to synthesize a functionalized polymer *via* cyanide substitution of the alkyl bromide on **PF-Br**. Initially, we reacted **PF-Br** (in THF) in the presence of potassium cyanide (KCN) in dimethyl formamide (Scheme 7). The reaction was unsuccessful as there was no observed shift of the methylene group protons adjacent to the bromide in **PF-Br** by ^{1}H-NMR spectroscopy. We hypothesized that the cyanide ion was

poorly soluble in the organic phase and as a result the substitution reaction did not occur. Alternatively, we dissolved the potassium cyanide in water, added tetrabutyl ammonium bromide ($^{n}Bu_4NBr$) and attempted a phase-transfer cyanide substitution with **PF-Br** in various organic solvents (Scheme 7). Again, no reaction was observed by ^{1}H-NMR spectroscopy. It is possible that the tetrabutyl ammonium bromide ion pair is more lipophilic than tetrabutyl ammonium cyanide, thus the cyanide nucleophile does not readily substitute the bromide in the organic phase.[176] Instead, we performed the alkylation employing tetrabutylammonium hydroxide TBAOH, which is exceedingly less lipophilic than the tetrabutylammonium cyanide ion,[176] allowing for facile substitution of the bromide in the organic phase. Reaction of **PF-Br** under these conditions yielded an insoluble product that could not be characterized by ^{1}H-NMR spectroscopy.
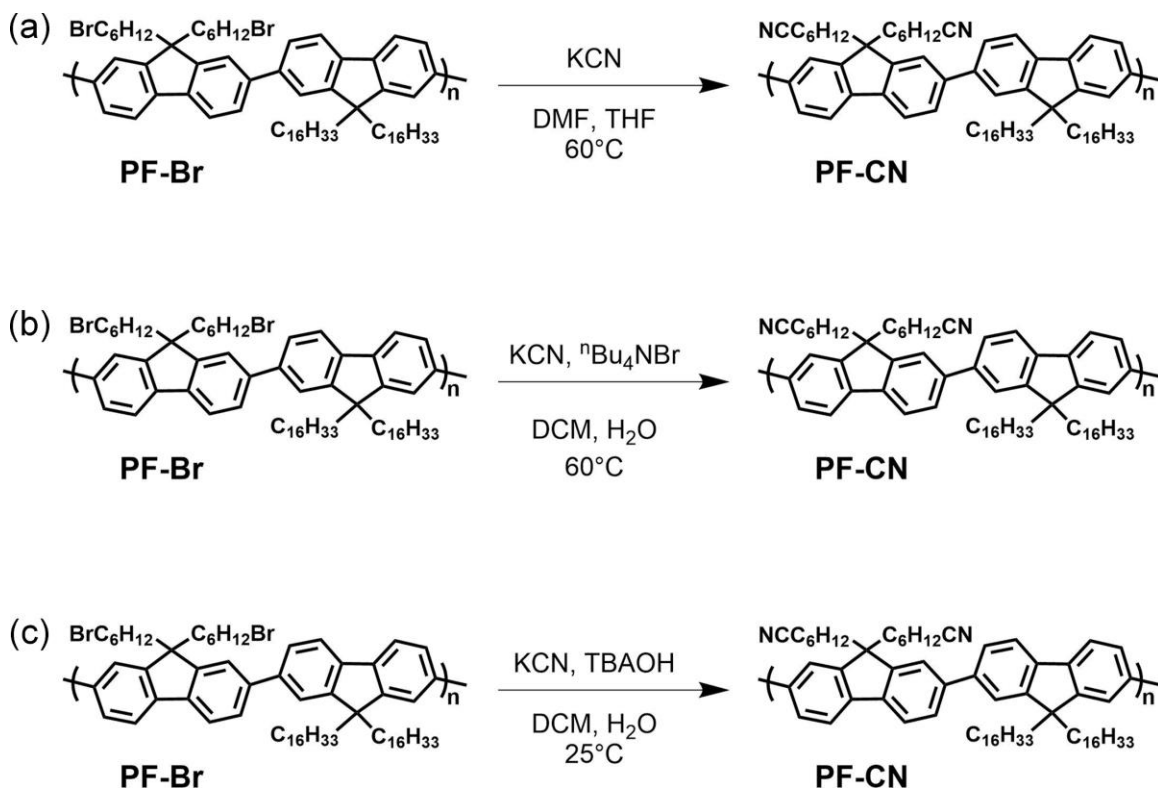
Scheme 7. Various attempts to synthesize polyfluorene containing alkyl nitrile side chains (**PF-CN**) via cyanide substitution of the alkyl bromide on polyfluorene bromide (**PF-Br**).

We were unsuccessful in our attempts to make **PF-CN**, and instead chose a homobifunctional PEG polymer with terminal alkyl nitriles (PEG_{600}-$(CN)_2$) to act as a crosslinker. We recently reported the synthesis of PEG_{600}-$(CN)_2$ in good yield from commercially available PEG_{600} and dibromohexane, which formed relatively soft organogels.[166]

Thus, to prepare the organogels, we first synthesized PEG_{600}-$(CN)_2$ to act as a crosslinker, according to literature procedures.[166] Figure 18 depicts an idealized cartoon representation of the supramolecular gel. We envisioned a system where the pillar[5]arene units interact with the alkyl nitrile groups in the PEG_{600}-$(CN)_2$ crosslinker to form a uniform crosslinked network.
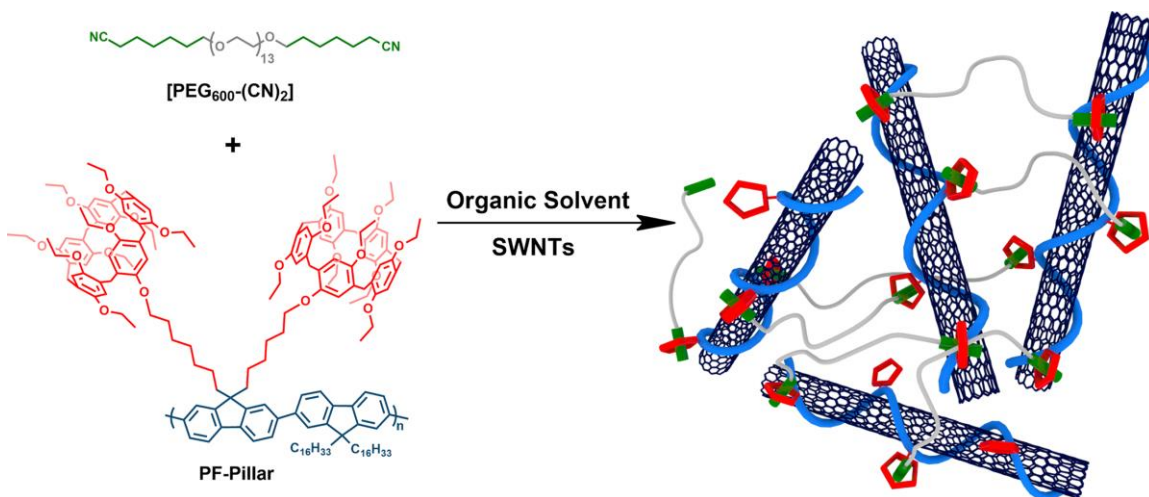
Figure 18. Cartoon representation of host-guest driven gelation of **PF-Pillar**-SWNT (red) and PEG$_{600}$-(CN)$_2$ (green).

3.2. Preparation of Organogels Utilising Solvent Exchange Method

We attempted to characterize the mechanical properties of the supramolecular organogels. With the organogel successfully made, we sought to explore the effect of added SWNTs on the stiffness of the gel. The Young's Modulus was determined by performing mechanical strength measurements on native (control) and hybrid organogels. Our initial mechanical testing of gels swollen with THF proved to be problematic due to the rapid evaporation of the organic solvent. This made the gels stiffer as the measurement progressed and resulted in inconsistent data.

To mitigate the problem of THF evaporation, we explored alternative low-boiling solvents when preforming mechanical strength testing of the gels. Attempts to make polymer-SWNT complexes in solvents such as toluene, xylene, chlorobenzene and 1,2-dichlorobenzene were unsuccessful, as the resultant dispersions were either too dilute or unstable (i.e. SWNT bundles formed immediately after centrifugation). A solvent exchange

method was employed to achieve a stable dispersion in a high boiling solvent such as 1,2-dichlorobenzene. Briefly, 100 µL of **PF-Pillar**-SWNT suspension in THF was added to 100 µL of 1,2-dichlorobenzene in a 20-mL vial. The mixture was placed under vacuum to evaporate the THF, resulting in a black **PF-Pillar-**SWNT dispersion in 1,2-dichlorobenzene.

To investigate any potential increase in bundling upon solvent exchange, Raman spectroscopy was preformed on thin film samples of SWNT dispersions in THF and 1,2-dichlorobenzene. Samples were prepared by drop-casting the dispersions onto silicon wafers. A laser excitation wavelength of 785 nm was used to characterize the samples. A reference sample containing only raw SWNTs was prepared *via* sonication in chloroform and drop-casting onto a silicon wafer. Figure 19 shows the radial breathing mode (RBM) region of the Raman spectra for **PF-Pillar**-SWNT dispersions cast from THF and 1,2-dichlorobenzene (full Raman spectra are provided in Figure S6). The spectra were normalized to the G-band at ~ 1590 cm^{-1} and offset for clarity. For HiPCO SWNTs at 785 nm, a prominent peak at 265 cm^{-1} arises from the (10,2) sc-SWNT chirality when bundled. This "bundling peak" may be used to identify the degree of bundling in a nanotube sample, assuming (10,2) is present.[177] The samples show a significant suppression of the bundling peak when HiPCO SWNTs were dispersed with **PF-Pillar** in THF. The degree of bundling was quantified by integrating the bundling peak (252 – 280 cm^{-1}) relative to the SWNT peaks (208 – 248 cm^{-1}) and comparing the relative intensities (integrations are tabulated in Table 1). Upon solvent exchange with 1,2-dichlorobenzene (by removing THF), the bundling peak intensity remained identical to the **PF-Pillar**-SWNT in THF (Table 1). To

corroborate the results of the Raman experiment, we recorded a PL map to confirm the presence of (10,2) sc-SWNTs. The PL map of **PF-Pillar**-SWNT (Figure 15, Section 2.4) shows a moderate intensity PL signal corresponding to (10,2) sc-SWNTs in the polymer-SWNT sample. As (10,2) is present, we can confirm that the Raman bundling analysis above is valid.[74]
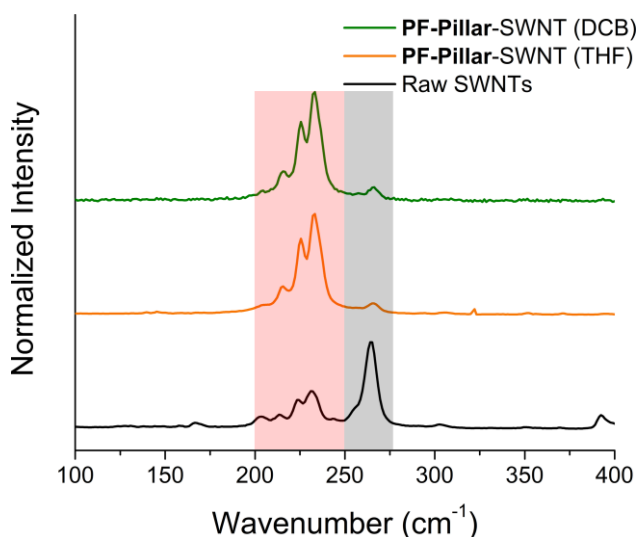
Figure 19. RBM regions of the Raman spectra of **PF-Pillar**-SWNT samples in THF and upon solvent exchange into 1,2-dichlorobenzene (DCB), compared with raw HiPCO SWNTs. The gray and pink boxes denote the regions of integrated bundling peaks and other SWNT chirlaities, respectively. The spectra were collected at 785 nm excitation wavelength, normalized to the G-band at ~1590 cm^{-1} and offset for clarity.

Table 1. Raman integration values of SWNT (208-248 cm^{-1}) and Bundling Peak (BP 252-280 cm^{-1}) of various SWNT dispersions and their relative ratios.

Name	SWNT (208-248 cm^{-1})	BP (252-280 cm^{-1})	SWNT: BP Ratio (Relative)[1]
PF-Pillar-SWNT (DCB)	7.9	0.3	100:4
PF-Pillar-SWNT (THF)	7.5	0.3	100:4
Raw SWNTs	2.3	2.7	100:116

1: Ratios were obtained through division of BP integrations by SWNT peak integration values and multiplication by 100.

Using this concept, we prepared 40 wt. % organogels in 1,2-dichlorobenzene by adding $PEG_{600}\text{-}(CN)_2$ crosslinker to the **PF-Pillar**-SWNT dispersion. The organogel samples were prepared inside a 2 mL microcentrifuge tube and incubated under ambient conditions for 30 min before inversion. The native organogel was prepared by combining **PF-Pillar** (22 mg, 8.2 µmol) with $PEG_{600}\text{-}(CN)_2$ (7 mg, 8.2 µmol) in 1,2-dichlorobenzene (50 µL). The hybrid, SWNT-containing organogel was prepared by first taking an aliquot of the pristine **PF-Pillar**-SWNT dispersion, adding the same volume of 1,2-dichlorobenzene, and then removing the THF *in vacuo*. The control organogel was prepared by combining **PF-Pillar** (22 mg, 8.2 µmol) to PEG_{600} (7 mg, 8.2 µmol) in 1,2-dichlorobenzene (50 µL).

After 30 minutes of incubation under ambient conditions, both the **PF-Pillar**-$PEG_{600}\text{-}(CN)_2$ (native) and **PF-Pillar**-SWNT-$PEG_{600}\text{-}(CN)_2$ (hybrid) mixtures formed gels that did not flow when the microcentrifuge tube was inverted, as shown in Figure 20. The resultant gels were soft and tacky in texture, with a marked difference in colour between the native (yellow) and hybrid (black) gels. In a control experiment, **PF-Pillar** and PEG_{600} were mixed in 1,2-dichlorobenzene under conditions identical to those used to form the aforementioned organogels. Upon inversion, this control mixture remained liquid and flowed down the wall of the container (Figure 20).
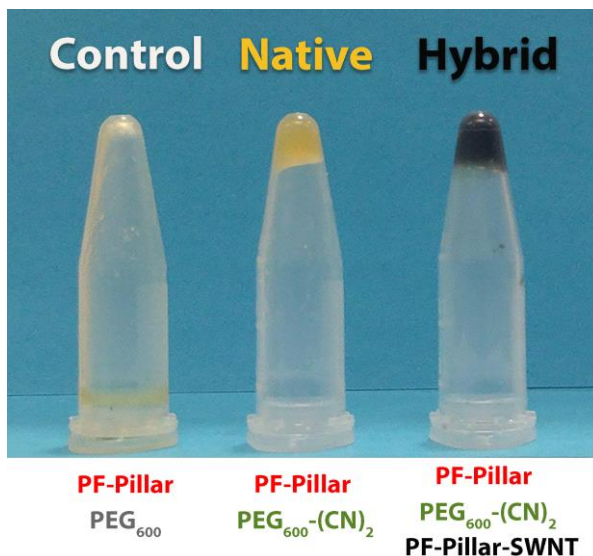
Figure 20. Photographs of supramolecular organogels made from the host-guest interaction between **PF-Pillar** and PEG600-(CN)$_2$ (native) and in the presence of SWNTs (hybrid).

3.3. Mechanical Testing of Organogels Utilising the CellScale Microsquisher

Having confirmed the formation of a supramolecular organogel in the presence of the **PF-Pillar**-SWNT dispersion, we sought to investigate the mechanical properties of the native and hybrid gels. The mechanical testing of the native and hybrid organogels was initially attempted with a CellScale Microsquisher at 22°C. This instrument is designed to apply a compressive load to specimens 50 to 2000 µm in size.[178] Organogel samples were prepared inside a modified 1 mL polypropylene syringe and allowed to incubate for 20 minutes before extruding into a round Teflon mold (4 mm diameter and 3 mm deep) for mechanical testing.

Figure 21 shows a photograph of the CellScale Microsquisher with the following major components: the microbeam, actuators, imaging system, and the fluid bath. The

microbeam is a circular tungsten beam with a Modulus of 411000 MPa and is available in a variety of diameters, ranging from 0.0762 to 0.5588 µm.[178] At the end of the microbeam shaft is a rigidly attached compression plate (or a stainless-steel ball may also be attached). The microbeam is rigidly fixed to the actuator, which aids in positioning the microbeam above a specimen. Then, the microbeam applies a deformation to the specimen while measuring the applied force. The applied force is determined by calculating the deflection of the microbeam (difference between the displacement of the tip and the displacement of the actuator). The deformation of the sample is monitored with an imaging system that is composed of a digital camera. The fluid bath is utilized for specialized temperature testing of samples.[178] This feature was not utilized in the testing of the supramolecular organogels considering that we sought to determine the mechanical properties at room temperature.
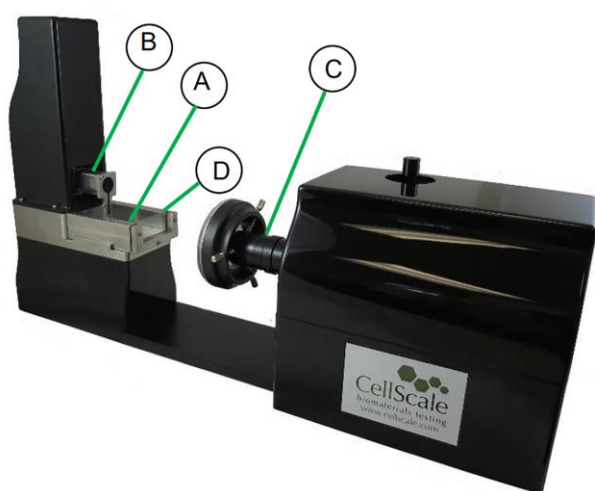
Figure 21. Photograph of the CellScale Microsquisher. Adapted from [CellScale. MicroSquisher Micro-scale Tension-Compression Test System].[178]

Figure 22 illustrates a typical test sequence achieved upon the application and release of a load on the specimen using the Microsquisher. The test sequence may be composed of numerous sets of test cycles. Each test cycle may be divided into the load, hold, recover, and rest phase.[178] The load phase encompasses the applied deformation to the specimen. The deformation may be expressed either in terms of the force applied or the displacement achieved. Upon completion of the load phase, the deformation is held on the specimen for a desired period of time. The recovery phase begins upon removal of the applied force onto the specimen. The recovery phase is followed by the rest phase, which is the time between the end of one cycle and the beginning of the next. The duration of the various test phases is configurable and dependent on the nature of the testing.[178]
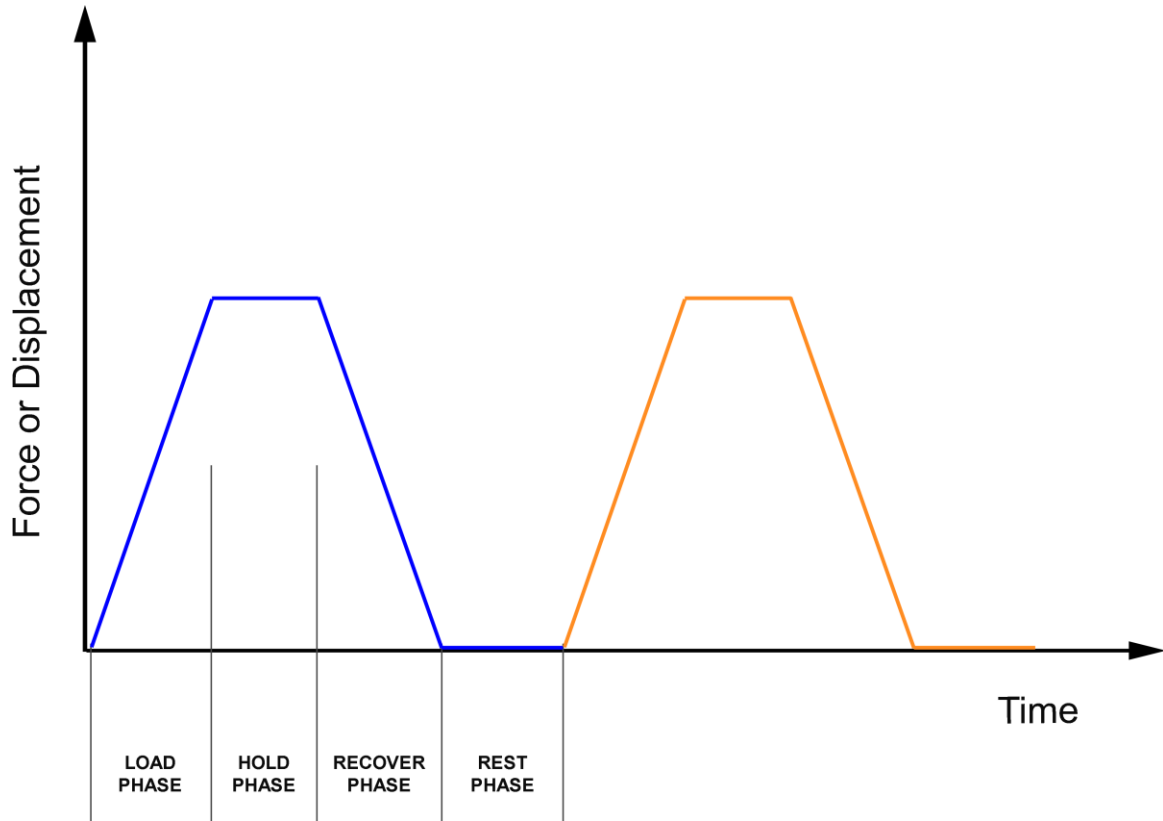
Figure 22. Test sequence showing the load, hold, recover, and rest phases using the CellScale Microsquisher. Adapted from [CellScale. MicroSquisher Micro-scale Tension-Compression Test System].[178]

The stiffness values may then be calculated based on a modified Hertz model[179,180] using the following equations:

$$\emptyset = cos^{-1} \left[\frac{R-\delta}{R} \right] \qquad (4)$$

$$a = (R - \delta)\, tan\phi f(a) = \frac{2(1+v)R^2}{(a^2+4R^2)^{3/2}} + \frac{1-v^2}{(a^2+4R^2)^{1/2}} \qquad (5)$$

$$E = \frac{3(1-v^2)F}{(4\delta a)} - \frac{f(a)F}{\pi\delta} \qquad (6)$$

Where F is the applied force, R is the sphere radius, δ is the displacement, v is the Poisson's ratio (0.5) and E is the Young's Modulus. The stiffness values are calculated using force and displacement values at an indentation of 10% of the indenter radius.[179]

To test the mechanical properties of the organogels, a compression probe was constructed by gluing a 3 mm diameter stainless steel ball to a 0.3048 µm diameter cantilever. The organogel samples were prepared inside a modified 1 mL polypropylene syringe and allowed to gel for 30 minutes before extruding into a round Teflon mold (4 mm diameter and 3 mm deep) for mechanical testing. Native organogels were prepared by combining equimolar ratios of **PF-Pillar** to PEG_{600}-$(CN)_2$ in 50 µL of 1,2-dichlorobenzene. Hybridized gels were prepared by mixing equimolar ratios of **PF-Pillar** to PEG_{600}-$(CN)_2$ in 50 µL of **PF-Pillar**-SWNT in 1,2-dichlorobenzene.

The organogel samples were indented using the MicroSquisher with a 3 mm stainless steel ball fixed to the end of the cantilever. The ball was indented into the gel by more than 0.3 mm in 60 seconds while collecting data at 1Hz. However, during the load phase, the indenter became stuck to the tacky gel, resulting in failure of the test sequence with no useful data obtained. Attempts to reduce the stickiness of the gel involved addition of a drop of silicone oil to the gel surface in order to prevent the indenter from sticking to the gel. It was found that addition of silicone oil did not mitigate the problem, and the test sequence failure ensued. Another attempt involved reduction of the contact time during the load phase to minimize the negative effects due the gel's texture. However, the indenter remained stuck to the organogel samples and the issues of the load phase could not be mitigated.

3.4. Mechanical Testing of Organogels using a Home-built Apparatus

Given the drawbacks outlined for the CellScale Microsquisher, the mechanical properties of the organogels were measured by alternative means. A home-built apparatus was utilized (according to literature procedures[181]) to determine the Young's Modulus of the **PF-Pillar** and **PF-Pillar-**SWNT organogels. The instrument measures the contact mechanics between a glass hemisphere and an elastic organogel. This relationship can be described by Hertzian theory using equation 3:

$$F = \frac{4ER^{1/2}}{(1-v^2)} d^{3/2} \qquad (7)$$

Where F is force (N), d is deformation (mm), R is radius of the glass hemispherical indenter (mm), v is the Poisson's ratio and E is the Young's modulus (kPa) of the elastic substrate.[182] Each organogel was investigated using a compression method with a hemispherical indenter consisting of a glass melting point tube (VWR) with a hemispherical end (r = 0.83 mm) attached to a force transducer (Transducer Techniques, GSO series, 10 g full scale). The vertical position of the glass indenter was controlled with a servo motor, which contacts and indents the gel at a constant speed. The force transducer is then able to measure the force applied by the gel relative to time and vertical position of the indenter. This was repeated in triplicate at different positions for each organogel. The Young's modulus was obtained using the equation described by Hertzian theory, rearranged to isolate Young's modulus as the slope when plotting the measured $F(d)$. Poisson's ratio is assumed to be v = 0.45, based on polymer gels having similar mechanical properties to elastic, rubber-like materials.[183,184]

Mechanical testing of the **PF-Pillar** and **PF-Pillar**-SWNT organogels revealed Young's moduli of 6.0 ± 0.2 and 5.8 ± 1.3 kPa, respectively. We hypothesize that the wt. % of SWNT in the **PF-Pillar**-SWNT organogel may be too low to observe substantial differences in mechanical properties. Overall, we demonstrate that supramolecular organogels incorporating **PF-Pillar**-coated SWNTs can be produced, and that gelation is unaffected by the presence of SWNTs.

3.5. Summary

We prepared a SWNT-containing organogel by crosslinking a **PF-Pillar** enriched dispersion with PEG_{600}-$(CN)_2$ in THF. The initial mechanical testing of organogels in THF proved to be problematic, as rapid evaporation of the solvent led to inconsistent data. However, we found that employing a solvent exchange of **PF-Pillar**-SWNT dispersions in THF to 1,2-dichlorobenzene mitigated the problem of rapid solvent evaporation in the resultant gels. Utilising both Raman spectroscopy and PL mapping, we determined that solvent exchange methods did not increase bundling of the SWNTs in our dispersion. The mechanical testing of organogel samples was conducted using a home-built apparatus where it was found that the presence of SWNTs does not affect the Young's moduli of the gel.

Chapter 4: Conclusions

4.1.   Overall Conclusions

Single-walled carbon nanotubes are interesting allotropes of carbon that have unique structural, mechanical, optical and electronic properties. Control of single-walled carbon nanotube dispersion properties is of substantial interest to the scientific community. In this work, we sought to investigate the effect of a cavitand, the pillar[5]arene, on the dispersion properties of a polymer-nanotube complex. The electron-rich pillar[5]arene host is capable of forming inclusion complexes with electron-poor guests such as alkyl nitriles. Here, we demonstrate that a macrocycle-containing polyfluorene derivative can produce unusually concentrated polymer-SWNT dispersions. Utilizing the host-guest capability of pillar[5]arene, the polymer-nanotube complex was incorporated into a supramolecular organogel.

The synthesis of the pillar[5]arene-containing polyfluorene derivative was outlined in Chapter 2, where the quantitative alkylation of polyfluorene with mono-de-ethylated pillar[5]arene was confirmed by ^{1}H-NMR spectroscopy. We show that the facile modification of a polyfluorene backbone with a pillar[5]arene macrocycle has a significant impact on the polymer-SWNT dispersion properties. As evidenced by UV-Vis-NIR spectroscopy, the dispersion post-functionalization with a macrocycle was substantially more concentrated than the corresponding dispersion without the cavitand. It was found that the polyfluorene derivative improved the concentration of SWNTs ~30-fold, from 20 to 600 μg·mL^{-1}, as determined by TGA. Using Raman and fluorescence spectroscopy, it was determined that the initial polyfluorene derivative preferentially dispersed sc-SWNT

species, while the pillar[5]arene-decorated polyfluorene produced dispersions containing both sc- and m-SWNTs. The formation of an inclusion complex between pillar[5]arene and 1,6-dicyanohexane was confirmed in the presence of the macrocycle-containing polymer-SWNT complex.

In Chapter 3, the host-guest properties of the macrocycle-containing polymer-SWNT complex were further explored. Initially, we envisioned a crosslinked network of the pillar moieties with the alkyl nitrile side chains of a polyfluorene to form a "zipper-like" organogel. However, after several unsuccessful attempts to synthesize the akyl nitrile-functionalized polymer, we prepared a homobifunctional PEG polymer with terminal alkyl nitriles to act as a crosslinker. The polymer-SWNT dispersion was successfully incorporated into supramolecular organogels. The mechanical testing of organogel samples was conducted using a home-built apparatus where it was found that the presence of SWNTs does not affect the Young's moduli of the gel.

The most significant contribution from this thesis includes the effect a macrocycle-functionalized conjugated polymer on the dispersion of carbon nanotubes. It was found that incorporation of pillar[5]arene moieties in the side chains of polyfluorene had a significant impact on the populations of semiconducting and metallic nanotubes dispersed. This work shows that simple and facile incorporation of bulky pillar[5]arene structures in the side chains impart steric stabilization to the colloidal polymer-nanotube dispersion, resulting in a dispersion enriched with SWNTs. Thus, a simple modification of the conjugated polymer backbone can have a profound effect on the properties of the polymer-nanotube sample. In addition, we found that post-polymerization functionalization with the macrocycle yielded

concentrated polymer-SWNT dispersions. Therefore, we were able to investigate the host-guest properties of a polymer-SWNT complex using ^{1}H-NMR spectroscopy.

4.2.   Recommendations

The work presented in this thesis strictly involved the incorporation of pillar[5]arenes in the side chains of polyfluorene for the non-covalent functionalization of carbon nanotubes. While there are a few examples of calixarenes[185–187] used in the dispersion of SWNTs, the incorporation of other cavitands in conjugated polymer-SWNT complexes remain largely unexplored. It would be interesting to investigate the effect of other macrocycles on the dispersion properties of a polymer-nanotube complex. For instance, one would compare the relative SWNT concentration and nanotube species dispersed before and after cavitand-functionalization of a conjugated polymer. The results of these studies may be compared to those presented in this thesis to gain further understanding of the effects of macrocycles on the dispersion properties of conjugated polymer-SWNT complexes.

References

(1)   Krätschmer, W.; Lamb, L. D.; Fostiropoulos, K.; Huffman, D. R. *Nature* **1990**, *347* (6291), 354–358.

(2)   Iijima, S. *Nature* **1991**, *354* (6348), 56–58.

(3)   Tasis, D.; Tagmatarchis, N.; Bianco, A.; Prato, M. *Chem. Rev.* **2006**, *106* (3), 1105–1136.

(4)   Park, S.; Vosguerichian, M.; Bao, Z. *Nanoscale* **2013**, *5* (5), 1727.

(5)   Terrones, M. *Annu. Rev. Mater.Res* **2003**, *33*, 419–501.

(6)   Ajayan, P. M. *Chem. Rev.* **1999**, *99* (7), 1787–1800.

(7)   Saito, R.; Dresselhaus, G.; Dresselhaus, M. *Physical Properties of Carbon Nanotubes*; 1998.

(8)   Coleman, J. N.; Khan, U.; Blau, W. J.; Gun'ko, Y. K. *Carbon* **2006**, *44* (9), 1624–1652.

(9)   Zhang, Q.; Huang, J.-Q.; Qian, W.-Z.; Zhang, Y.-Y.; Wei, F. *Small* **2013**, *9* (8), 1237–1265.

(10)   O'Connell, M. J.; Bachilo, S. M.; Huffman, C. B.; Moore, V. C.; Strano, M. S.; Haroz, E. H.; Rialon, K. L.; Boul, P. J.; Noon, W. H.; Kittrell, C.; Ma, J.; Hauge, R. H.; Weisman, R. B.; Smalley, R. E. *Science* **2002**, *297* (5581), 593–596.

(11)   Bachilo, S. M.; Strano, M. S.; Kittrell, C.; Hauge, R. H.; Smalley, R. E.; Weisman, R. B. *Science* **2002**, *298* (5602), 2361–2366.

(12)   Kataura, H.; Kumazawa, Y.; Maniwa, Y.; Umezu, I.; Suzuki, S.; Ohtsuka, Y.; Achiba, Y. *Synth. Met.* **1999**, *103* (1–3), 2555–2558.

(13)   Rice, N. A. Separation of Single-Walled Carbon Nanotubes By Electronic Type Using Conjugated Polymers, McMaster University, 2015.

(14)   Bhushan, B. *Springer Handbook of Nanotechnology*; Bhushan, B., Ed.; Springer US, 2004.

(15)   Balasubramanian, K.; Burghard, M. *Small* **2005**, *1* (2), 180–192.

(16)   Chen, F.; Wang, B.; Chen, Y.; Li, L. J. *Nano Lett.* **2007**, *7* (10), 3013–3017.

(17)   Rafique, M. M. A.; Iqbal, J. *J. Encapsulation Adsorpt. Sci.* **2011**, *1*, 29–34.

(18)   Guo, T.; Nikolaev, P.; Thess, A.; Colbert, D. T.; Smalley, R. E. *Chem. Phys. Lett.* **1995**, *243* (1–2), 49–54.

(19)   Scott, C. D.; Arepalli, S.; Nikolaev, P.; Smalley, R. E. *Appl. Phys. A Mater. Sci. Process.* **2001**, *72* (5), 573–580.

(20)   Li, W. Z.; Xie, S. S.; Qian, L. X.; Chang, B. H.; Zou, B. S.; Zhou, W. Y.; Zhao, R. A.; Wang, G. *Science* **1996**, *274* (5293), 1701–1703.

(21)   Chiang, I. W.; Brinson, B. E.; Huang, A. Y.; Willis, P. A.; Bronikowski, M. J.; Margrave, J. L.; Smalley, R. E.; Hauge, R. H. *J. Phys. Chem. B* **2001**, *105* (35), 8297–8301.

(22)   Resasco, D. E.; Alvarez, W. E.; Pompeo, F.; Balzano, L.; Herrera, J. E.; Kitiyanan, B.; Borgna, A. *J. Nanoparticle Res.* **2002**, *4* (1/2), 131–136.

(23)   Nikolaev, P.; Bronikowski, M. J.; Bradley, R. K.; Rohmund, F.; Colbert, D. T.; Smith, K. .; Smalley, R. E. *Chem. Phys. Lett.* **1999**, *313* (1–2), 91–97.

(24)   Kong, J.; Cassell, A. M.; Dai, H. *Chem. Phys. Lett.* **1998**, *292* (4–6), 567–574.

(25)   Journet, C.; Maser, W. K.; Bernier, P.; Loiseau, A.; de la Chapelle, M. L.; Lefrant,

S.; Deniard, P.; Lee, R.; Fischer, J. E. *Nature* **1997**, *388* (6644), 756–758.

(26) Guo, T.; Nikolaev, P.; Thess, A.; Colbert, D. T.; Smalley, R. E. *Chem. Phys. Lett.* **1995**, *243* (1–2), 49–54.

(27) Kim, K. S.; Cota-Sanchez, G.; Kingston, C. T.; Imris, M.; Simard, B.; Soucy, G. *J. Phys. D. Appl. Phys.* **2007**, *40* (8), 2375–2387.

(28) Campidelli, S.; Klumpp, C.; Bianco, A.; Guldi, D. M.; Prato, M. *J. Phys. Org. Chem.* **2006**, *19* (8–9), 531–539.

(29) Britz, D. A.; Khlobystov, A. N. *Chem. Soc. Rev.* **2006**, *35* (7), 637.

(30) Hirsch, A. *Angew. Chemie - Int. Ed.* **2002**, *41* (11), 1853–1859.

(31) Li, H.; Cheng, F.; Duft, A. M.; Adronov, A. *J. Am. Chem. Soc.* **2005**, *127* (41), 14518–14524.

(32) Liu, J.; Rinzler, A. G.; Dai, H.; Hafner, J. H.; Kelley Bradley, R.; Boul, P. J.; Lu, A.; Iverson, T.; Shelimov, K.; Huffman, C. B.; Rodriguez-Macias, F.; Shon, Y. S.; Lee, T. R.; Colbert, D. T.; Smalley, R. E. *Science* **1998**, *280* (5367), 1253–1256.

(33) Gavrel, G.; Jousselme, B.; Filoramo, A.; Campidelli, S. Springer, Berlin, Heidelberg, 2013; pp 95–126.

(34) Bilalis, P.; Katsigiannopoulos, D.; Avgeropoulos, A.; Sakellariou, G. *RSC Adv.* **2014**, *4* (6), 2911–2934.

(35) Gong, X.; Liu, J.; Baskaran, S.; Voise, R. D.; Young, J. S. *Chem. Mater.* **2000**, *12* (4), 1049–1052.

(36) Islam, M. F.; Rojas, E.; Bergey, D. M.; Johnson, A. T.; Yodh, A. G. *Nano Lett.* **2003**, *3* (2), 269–273.

(37)   Moore, V. C.; Strano, M. S.; Haroz, E. H.; Hauge, R. H.; Smalley, R. E.; Schmidt, J.; Talmon, Y. *Nano Lett.* **2003**, *3* (10), 1379–1382.

(38)   Chen, R. J.; Zhang, Y.; Wang, D.; Dai, H. *Science* **2001**, *123* (16), 3838–3839.

(39)   Tomonari, Y.; Murakami, H.; Nakashima, N. *Chem. - A Eur. J.* **2006**, *12* (15), 4027–4034.

(40)   Yang, K.; Zhu, L.; Xing, B. *Environ. Sci. Technol.* **2006**, *40* (6), 1855–1861.

(41)   Nish, A.; Hwang, J.-Y.; Doig, J.; Nicholas, R. J. *Nat. Nanotechnol.* **2007**, *2* (10), 640.

(42)   Star, A.; Stoddart, J. F.; Steuerman, D.; Diehl, M.; Boukai, A.; Wong, E. W.; Yang, X.; Chung, S.-W.; Choi, H.; Heath, J. R. *Angew. Chemie - Int. Ed.* **2001**, *40* (9), 1721–1725.

(43)   Nish, A.; Hwang, J.-Y.; Doig, J.; Nicholas, R. J. *Nat. Nanotechnol.* **2007**, *2* (10), 640–646.

(44)   Heller, D. A.; Jeng, E. S.; Yeung, T.-K.; Martinez, B. M.; Moll, A. E.; Gastala, J. B.; Strano, M. S. *Science* **2006**, *311* (5760), 508–511.

(45)   Zheng, M.; Jagota, A.; Semke, E. D.; Diner, B. A.; Mclean, R. S.; Lustig, S. R.; Richardson, R. E.; Tassi, N. G. *Nat. Mater.* **2003**, *2* (5), 338–342.

(46)   Zheng, M.; Jagota, A.; Strano, M. S.; Santos, A. P.; Barone, P.; Chou, S. G.; Diner, B. A.; Dresselhaus, M. S.; McLean, R. S.; Onoa, G. B.; Samsonidze, G. G.; Semke, E. D.; Usrey, M.; Walls, D. J. *Science* **2003**, *302* (5650), 1545–1548.

(47)   Bradley, K.; Briman, M.; Star, A.; Gruner, G. *Nano Lett.* **2004**, *4* (2), 253–256.

(48)   Balavoine, F.; Schultz, P.; Richard, C.; Mallouh, V.; Ebbesen, T. W.; Mioskowski,

C. *Angew. Chemie - Int. Ed.* **1999**, *38* (13–14), 1912–1915.

(49) Guo, Z.; Sadler, P. J.; Tsang, S. C. *Adv. Mater.* **1998**, *10* (9), 701–703.

(50) Moore, V. C.; Strano, M. S.; Haroz, E. H.; Hauge, R. H.; Smalley, R. E.; Schmidt, J.; Talmon, Y. *Nano Lett.* **2003**, *3* (10), 1379–1382.

(51) Blanch, A. J.; Lenehan, C. E.; Quinton, J. S. *J. Phys. Chem. B* **2010**, *114* (30), 9805–9811.

(52) Arnold, M. S.; Green, A. A.; Hulvat, J. F.; Stupp, S. I.; Hersam, M. C. *Nat. Nano.* **2006**, *1* (1), 60.

(53) Graham, J. M. *Biological Centrifugation (The Basics)*; BIOS Scientific: Milton Park, 2001.

(54) Hersam, M. C. *Nature Nanotechnology*. Nature Publishing Group July 30, 2008, pp 387–394.

(55) Miyata, Y.; Yanagi, K.; Maniwa, Y.; Kataura, H. *J. Phys. Chem. C* **2008**, *112* (10), 3591–3596.

(56) Crochet, J.; Clemens, M.; Hertel, T. *J. Am. Chem. Soc.* **2007**, *129* (26), 8058–8059.

(57) Backes, C.; Hauke, F.; Schmidt, C. D.; Hirsch, A. *Chem. Commun.* **2009**, *0* (19), 2643–2645.

(58) Green, A. A.; Hersam, M. C. *Nano Lett.* **2008**, *8* (5), 1417–1422.

(59) Ghosh, S.; Bachilo, S. M.; Weisman, R. B. *Nat. Nanotechnol.* **2010**, *5* (6), 443–450.

(60) Jung, S.; Cha, M.; Park, J.; Jeong, N.; Kim, G.; Park, C.; Ihm, J.; Lee, J. *J. Am. Chem. Soc.* **2010**, *132* (32), 10964–10966.

(61)   Tu, X.; Manohar, S.; Jagota, A.; Zheng, M. *Nature* **2009**, *460* (7252), 250–253.

(62)   Woo, H. S.; Czerw, R.; Webster, S.; Carroll, D. L.; Ballato, J.; Strevens, A. E.; O'Brien, D.; Blau, W. J. *Appl. Phys. Lett.* **2000**, *77* (9), 1393–1395.

(63)   Steuerman, D. W.; Star, A.; Narizzano, R.; Choi, H.; Ries, R. S.; Nicolini, C.; Stoddart, J. F.; Heath, J. R. *J. Phys. Chem. B* **2002**, *106* (12), 3124–3130.

(64)   Chen, J.; Liu, H.; Weimer, W. A.; Halls, M. D.; Waldeck, D. H.; Walker, G. C. *J. Am. Chem. Soc.* **2002**, *124* (31), 9034–9035.

(65)   Bilalis, P.; Katsigiannopoulos, D.; Avgeropoulos, A.; Sakellariou, G. *RSC Adv.* **2014**, *4* (6), 2911–2934.

(66)   Gomulya, W.; Gaoa, J.; Loib, M. A. *Eur. Phys. J. B* **2013**, *86* (10), 404.

(67)   Zhang, D.; Yang, J.; Li, Y. *Small* **2013**, *9* (8), 1284–1304.

(68)   Cheng, F.; Imin, P.; Maunders, C.; Botton, G.; Adronov, A. *Macromolecules* **2008**, *41* (7), 2304–2308.

(69)   O'Connell, M. J.; Bachilo, S. M.; Huffman, C. B.; Moore, V. C.; Strano, M. S.; Haroz, E. H.; Rialon, K. L.; Boul, P. J.; Noon, W. H.; Kittrell, C.; Ma, J.; Hauge, R. H.; Weisman, R. B.; Smalley, R. E. *Science* **2002**, *297* (5581), 593–596.

(70)   O'Connell, M. J.; Bachilo, S. M.; Huffman, C. B.; Moore, V. C.; Strano, M. S.; Haroz, E. H.; Rialon, K. L.; Boul, P. J.; Noon, W. H.; Kittrell, C.; Ma, J.; Hauge, R. H.; Weisman, R. B.; Smalley, R. E. *Science* **2002**, *297* (5581), 593–596.

(71)   Strano, M. S.; Dyke, C. A.; Usrey, M. L.; Barone, P. W.; Allen, M. J.; Shan, H.; Kittrell, C.; Hauge, R. H.; Tour, J. M.; Smalley, R. E. *Science* **2003**, *301* (2003), 1519–1522.

(72) Luo, Z.; Pfefferle, L. D.; Haller, G. L.; Papadimitrakopoulos, F. *J. Am. Chem. Soc.* **2006**, *128* (48), 15511–15516.

(73) Bachilo, S. M.; Strano, M. S.; Kittrell, C.; Hauge, R. H.; Smalley, R. E.; Weisman, R. B. *Science* **2002**, *298* (5602), 2361–2366.

(74) R. Bruce Weisman*; Bachilo, S. M. *Nano Lett.* **2003**, *3* (9), 1235–1238.

(75) Kataura, H.; Kumazawa, Y.; Maniwa, Y.; Umezu, I.; Suzuki, S.; Ohtsuka, Y.; Achiba, Y. *Synth. Met.* **1999**, *103* (1–3), 2555–2558.

(76) Ohno, Y.; Maruyama, S.; Mizutani, T. **1998**, 109–123.

(77) Michel, T.; Paillet, M.; Nakabayashi, D.; Picher, M.; Jourdain, V.; Meyer, J. C.; Zahab, A. A.; Sauvajol, J. L. *Phys. Rev. B - Condens. Matter Mater. Phys.* **2009**, *80* (24), 245416.

(78) Fantini, C.; Jorio, A.; Santos, A. P.; Peressinotto, V. S. T.; Pimenta, M. A. *Chem. Phys. Lett.* **2007**, *439* (1–3), 138–142.

(79) Dresselhaus, M. S.; Dresselhaus, G.; Jorio, A.; Souza Filho, A. G.; Pimenta, M. A.; Saito, R. *Acc. Chem. Res.* **2002**, *35* (12), 1070–1078.

(80) Sato, K.; Saito, R.; Jiang, J.; Dresselhaus, G.; Dresselhaus, M. S. *Phys. Rev. B - Condens. Matter Mater. Phys.* **2007**, *76* (19), 195446.

(81) Nugraha, A. R. T.; Saito, R.; Sato, K.; Araujo, P. T.; Jorio, A.; Dresselhaus, M. S. *Appl. Phys. Lett.* **2010**, *97* (9), 091905.

(82) Rao, A. M.; Richter, E.; Bandow, S.; Chase, B.; Eklund, P. C.; Williams, K. A.; Fang, S.; Subbaswamy, K. R.; Menon, M.; Thess, A.; Smalley, R. E.; Dresselhaus, G.; Dresselhaus, M. S. *Science* **1997**, *275* (5297), 187–190.

(83)   Dresselhaus, M. S.; Dresselhaus, G.; Saito, R.; Jorio, A. *Phys. Rep.* **2005**, *409* (2), 47.

(84)   Garrett, M.; Ivanov, I. N.; Geohegan, D.; Hu, B. *Carbon* **2013**, *64*, 1–5.

(85)   Park, T. J.; Banerjee, S.; Hemraj-Benny, T.; Wong, S. S. *J. Mater. Chem.* **2006**, *16* (2), 141–154.

(86)   Brown, S. D. M.; Jorio, A.; Corio, P.; Dresselhaus, M. S.; Dresselhaus, G.; Saito, R.; Kneipp, K. *Phys. Rev. B - Condens. Matter Mater. Phys.* **2001**, *63* (15), 155414.

(87)   Lehn, J. -M. *Angew. Chemie - Int. Ed.* **1988**, *27* (1), 89–112.

(88)   Cram, D. J. *Angewandte Chemie International Edition in English*. Wiley-Blackwell August 1, 1988, pp 1009–1020.

(89)   Pedersen, C. J. *Angewandte Chemie International Edition in English*. Wiley-Blackwell August 1, 1988, pp 1021–1027.

(90)   Steed, K.; Turner, D.; Wallace, K. *Core concepts in supramolecular chemistry and nanochemistry*; John Wiley & Sons, Ltd, 2007.

(91)   Chen, G.; Jiang, M. *Chemical Society Reviews*. Royal Society of Chemistry April 18, 2011, pp 2254–2266.

(92)   Szejtli, J. *Chem. Rev.* **1998**, *98* (5), 1743–1754.

(93)   Davis, M. E.; Brewster, M. E. *Nature Reviews Drug Discovery*. Nature Publishing Group December 1, 2004, pp 1023–1035.

(94)   Guo, D. S.; Liu, Y. *Chemical Society Reviews*. Royal Society of Chemistry August 20, 2012, pp 5907–5921.

(95)   Kim, J. S.; Quang, D. T. *Chemical Reviews*. American Chemical Society 2007, pp 3780–3799.

(96)   Rebek Jr., J. *Chem. Commun.* **2000**, *0* (8), 637–643.

(97)   Kim, K. *Chemical Society Reviews*. Royal Society of Chemistry March 18, 2002, pp 96–107.

(98)   Assaf, K. I.; Nau, W. M. *Chemical Society Reviews*. Royal Society of Chemistry December 22, 2015, pp 394–418.

(99)   Kim, K.; Selvapalam, N.; Ko, Y. H.; Park, K. M.; Kim, D.; Kim, J. *Chem. Soc. Rev.* **2007**, *36* (2), 267–279.

(100)   Ogoshi, T.; Shiga, R.; Hashizume, M.; Yamagishi, T. A. *Chem. Commun.* **2011**, *47* (24), 6927–6929.

(101)   Ogoshi, T.; Demachi, K.; Kitajima, K.; Yamagishi, T. A. *Chem. Commun.* **2011**, *47* (25), 7164–7166.

(102)   Ogoshi, T.; Kitajima, K.; Aoki, T.; Fujinami, S.; Yamagishi, T. A.; Nakamoto, Y. *J. Org. Chem.* **2010**, *75* (10), 3268–3273.

(103)   Ogoshi, T.; Kanai, S.; Fujinami, S.; Yamagishi, T.-A.; Nakamoto, Y. *J. Am. Chem. Soc.* **2008**, *130*, 5022–5023.

(104)   Strutt, N. L.; Zhang, H.; Giesener, M. A.; Lei, J.; Stoddart, J. F. *Chem. Commun.* **2012**, *48* (11), 1647–1649.

(105)   Ogoshi, T.; Hashizume, M.; Yamagishi, T. A.; Nakamoto, Y. *Chem. Commun.* **2010**, *46* (21), 3708–3710.

(106)   Ogoshi, T.; Nishida, Y.; Yamagishi, T. A.; Nakamoto, Y. *Macromolecules* **2010**,

43 (7), 3145–3147.

(107) Deng, H.; Shu, X.; Hu, X.; Li, J.; Jia, X.; Li, C. *Tetrahedron Lett.* **2012**, *53* (34), 4609–4612.

(108) Strutt, N. L.; Forgan, R. S.; Spruell, J. M.; Botros, Y. Y.; Stoddart, J. F. *J. Am. Chem. Soc.* **2011**, *133* (15), 5668–5671.

(109) Shu, X.; Chen, S.; Li, J.; Chen, Z.; Weng, L.; Jia, X.; Li, C. *Chem. Commun.* **2012**, *48* (24), 2967.

(110) Li, Z. Y.; Zhang, Y.; Zhang, C. W.; Chen, L. J.; Wang, C.; Tan, H.; Yu, Y.; Li, X.; Yang, H. B. *J. Am. Chem. Soc.* **2014**, *136* (24), 8577–8589.

(111) Ye, F.; Wei, R.; Wang, L.; Meier, H.; Cao, D. *RSC Adv.* **2016**, *6* (92), 89810–89814.

(112) Ogoshi, T.; Nishida, Y.; Yamagishi, T.; Nakamoto, Y. *Macromolecules* **2010**, *43* (7), 3145–3147.

(113) Ogoshi, T.; Nishida, Y.; Yamagishi, T.; Nakamoto, Y. *Macromolecules* **2010**, *43* (17), 7068–7072.

(114) Ogoshi, T.; Hasegawa, Y.; Aoki, T.; Ishimori, Y.; Inagi, S.; Yamagishi, T. *Macromolecules* **2011**, *44* (19), 7639–7644.

(115) Sun, S.; Hu, X. Y.; Chen, D.; Shi, J.; Dong, Y.; Lin, C.; Pan, Y.; Wang, L. *Polym. Chem.* **2013**, *4* (7), 2224–2229.

(116) Wang, P.; Yao, Y.; Xue, M. *Chem. Commun.* **2014**, *50* (39), 5064–5067.

(117) Ogoshi, T.; Aoki, T.; Ueda, S.; Tamura, Y.; Yamagishi, T. *Chem. Commun.* **2014**, *50* (50), 6607–6609.

(118) Chang, J.; Zhao, Q.; Kang, L.; Li, H.; Xie, M.; Liao, X. *Macromolecules* **2016**, *49* (7), 2814–2820.

(119) Gribble, G. W.; Nutaitis, C. F. *Tetrahedron Lett.* **1985**, *26* (49), 6023–6026.

(120) Gutsche, C. D. *Calixarenes Revisited*; 1998.

(121) Patrick, T. B.; Egan, P. A. *Journal of Organic Chemistry*. 1977, pp 382–383.

(122) Gutsche, C. D.; Muthukrishnan, R. *J. Org. Chem.* **1978**, *43* (25), 4905–4906.

(123) Rowan, S. J.; Cantrill, S. J.; Cousins, G. R. L.; Sanders, J. K. M.; Stoddart, J. F. *Angew. Chemie - Int. Ed.* **2002**, *41* (6), 898–952.

(124) Alexander, V. *Chem. Rev.* **1995**, *95*, 273–342.

(125) Holler, M.; Allenbach, N.; Sonet, J.; Nierengarten, J. F. *Chem. Commun.* **2012**, *48* (20), 2576–2578.

(126) Cragg, P. J.; Sharma, K. *Chemical Society Reviews*. Royal Society of Chemistry January 4, 2012, pp 597–607.

(127) Strutt, N. L.; Zhang, H.; Schneebeli, S. T.; Stoddart, J. F. *Acc. Chem. Res.* **2014**, *47* (8), 2631–2642.

(128) Strutt, N. L.; Zhang, H.; Giesener, M. A.; Lei, J.; Stoddart, J. F. *Chem. Commun.* **2012**, *48* (11), 1647–1649.

(129) Zhang, H.; Strutt, N. L.; Stoll, R. S.; Li, H.; Zhu, Z.; Stoddart, J. F. *Chem. Commun.* **2011**, *47* (41), 11420–11422.

(130) Zhang, H.; Ma, X.; Guo, J.; Nguyen, K. T.; Zhang, Q.; Wang, X. J.; Yan, H.; Zhu, L.; Zhao, Y. *RSC Adv.* **2013**, *3* (2), 368–371.

(131) Ogoshi, T.; Demachi, K.; Kitajima, K.; Yamagishi, T. A. *Chem. Commun.* **2011**,

47 (25), 7164–7166.

(132) Ogoshi, T.; Demachi, K.; Kitajima, K.; Yamagishi, T. *Chem. Commun.* **2011**, *47* (37), 10290.

(133) Chen, Y.; He, M.; Li, B.; Wang, L.; Meier, H.; Cao, D. *RSC Adv.* **2013**, *3* (44), 21405–21408.

(134) Ogoshi, T. *Pillararenes*; Ogoshi, T., Ed.; Royal Society of Chemistry, 2016.

(135) Ogoshi, T.; Kitajima, K.; Aoki, T.; Yamagishi, T. A.; Nakamoto, Y. *J. Phys. Chem. Lett.* **2010**, *1* (5), 817–821.

(136) Deng, H.; Shu, X.; Hu, X.; Li, J.; Jia, X.; Li, C. *Tetrahedron Lett.* **2012**, *53* (34), 4609–4612.

(137) Shu, X.; Chen, S.; Li, J.; Chen, Z.; Weng, L.; Jia, X.; Li, C. *Chem. Commun.* **2012**, *48* (24), 2967–2969.

(138) Shu, X.; Fan, J.; Li, J.; Wang, X.; Chen, W.; Jia, X.; Li, C. *Org. Biomol. Chem.* **2012**, *10* (17), 3393–3397.

(139) Thordarson, P. *Chemical Society Reviews*. 2011, pp 1305–1323.

(140) Liang, S.; Zhao, Y.; Adronov, A. *J. Am. Chem. Soc.* **2014**, *136* (3), 970–977.

(141) Pochorovski, I.; Wang, H.; Feldblyum, J. I.; Zhang, X.; Antaris, A. L.; Bao, Z. *J. Am. Chem. Soc.* **2015**, *137* (13), 4328–4331.

(142) Lei, T.; Pochorovski, I.; Bao, Z. *Acc. Chem. Res.* **2017**, *50* (4), 1096–1104.

(143) Lei, T.; Chen, X.; Pitner, G.; Wong, H.-S. P.; Bao, Z. *J. Am. Chem. Soc.* **2016**, *138* (3), 802–805.

(144) Toshimitsu, F.; Nakashima, N. *Nat. Commun.* **2014**, *5*, 5041.

(145) Fong, D.; Andrews, G. M.; McNelles, S. A.; Adronov, A. *Polym. Chem.* **2018**, *9* (35), 4460–4467.

(146) Fong, D.; Andrews, G. M.; Adronov, A. *Polym. Chem.* **2018**, *9* (21), 2873–2879.

(147) Fong, D.; Yeung, J.; McNelles, S. A.; Adronov, A. *Macromolecules* **2018**, *51* (3), 755–762.

(148) Driggers, E. M.; Hale, S. P.; Lee, J.; Terrett, N. K. *Nature Reviews Drug Discovery*. Nature Publishing Group July 1, 2008, pp 608–624.

(149) Heinis, C. *Nat. Chem. Biol.* **2014**, *10* (9), 696–698.

(150) Marsault, E.; Peterson, M. L. *J. Med. Chem.* **2011**, *54* (7), 1961–2004.

(151) Ogoshi, T.; Harada, A. *Sensors* **2008**, *8* (8), 4961–4982.

(152) Iyoda, M.; Yamakawa, J.; Rahman, M. J. *Angewandte Chemie - International Edition*. Wiley-Blackwell November 4, 2011, pp 10522–10553.

(153) Chen, Z.; Wang, Q.; Wu, X.; Li, Z.; Jiang, Y. B. *Chem. Soc. Rev.* **2015**, *44* (13), 4249–4263.

(154) Guo, D.-S.; Liu, Y. *Chem. Soc. Rev.* **2012**, *41* (18), 5907.

(155) Ogoshi, T.; Demachi, K.; Kitajima, K.; Yamagishi, T. A. *Chem. Commun.* **2011**, *47* (25), 7164–7166.

(156) Ogoshi, T.; Kitajima, K.; Aoki, T.; Fujinami, S.; Yamagishi, T. A.; Nakamoto, Y. *J. Org. Chem.* **2010**, *75* (10), 3268–3273.

(157) Chang, J.; Zhao, Q.; Kang, L.; Li, H.; Xie, M.; Liao, X. *Macromolecules* **2016**, *49* (7), 2814–2820.

(158) Rice, N. A.; Adronov, A. *Macromolecules* **2013**, *46* (10), 3850–3860.

(159) Fong, D.; Bodnaryk, W. J.; Rice, N. A.; Saem, S.; Moran-Mirabal, J. M.; Adronov, A. *Chem. - A Eur. J.* **2016**, *22* (41), 14560–14566.

(160) Lemasson, F.; Berton, N.; Tittmann, J.; Hennrich, F.; Kappes, M. M.; Mayor, M. *Macromolecules* **2012**, *45* (2), 713–722.

(161) Lemasson, F. A.; Strunk, T.; Gerstel, P.; Hennrich, F.; Lebedkin, S.; Barner-Kowollik, C.; Wenzel, W.; Kappes, M. M.; Mayor, M. *J. Am. Chem. Soc.* **2011**, *133* (4), 652–655.

(162) Strano, M. S.; Zheng, M.; Jagota, A.; Onoa, G. B.; Heller, D. A.; Barone, P. W.; Usrey, M. L. *Nano Lett.* **2004**, *4* (4), 543–550.

(163) Strano, M. S.; Doorn, S. K.; Haroz, E. H.; Kittrell, C.; Hauge, R. H.; Smalley, R. E. *Nano Lett.* **2003**, *3* (8), 1091–1096.

(164) Strano, M. S.; Dyke, C. A.; Usrey, M. L.; Barone, P. W.; Allen, M. J.; Shan, H.; Kittrell, C.; Hauge, R. H.; Tour, J. M.; Smalley, R. E. *Science* **2003**, *301* (5639), 1519–1522.

(165) Doorn, S. K.; Heller, D. A.; Barone, P. W.; Usrey, M. L.; Strano, M. S. *Appl. Phys. A Mater. Sci. Process.* **2004**, *78* (8), 1147–1155.

(166) Kardelis, V.; Li, K.; Nierengarten, I.; Holler, M.; Nierengarten, J. F.; Adronov, A. *Macromolecules* **2017**, *50* (23), 9144–9150.

(167) Chen, Q.; Zhu, L.; Zhao, C.; Wang, Q.; Zheng, J. *Adv. Mater.* **2013**, *25* (30), 4171–4176.

(168) Rong, Q.; Lei, W.; Chen, L.; Yin, Y.; Zhou, J.; Liu, M. *Angew. Chemie - Int. Ed.* **2017**.

(169) Coleman, J. N.; Khan, U.; Gun'ko, Y. K. *Adv. Mater.* **2006**, *18* (6), 689–706.

(170) Cadek, M.; Coleman, J. N.; Ryan, K. P.; Nicolosi, V.; Bister, G.; Fonseca, A.; Nagy, J. B.; Szostak, K.; Béguin, F.; Blau, W. J. *Nano Lett.* **2004**, *4* (2), 353–356.

(171) Baughman, R. H.; Zakhidov, A. A.; de Heer, W. A. *Science* **2002**, *297* (5582), 787–792.

(172) Coleman, J. N.; Khan, U.; Blau, W. J.; Gun'ko, Y. K. *Carbon* **2006**, *44* (9), 1624–1652.

(173) Ajayan, P. M.; Tour, J. M. *Nature* **2007**, *447* (7148), 1066–1068.

(174) Christopherson, D. G.; L Cox, B. H. *Appl. iMath. Soc. A* **1948**, *1* (165), 253–248.

(175) Treacy, M. M. J.; Ebbesen, T. W.; Gibson, J. M. *Nature* **1996**, *381* (6584), 678–680.

(176) Mastracchio, A. Phase-Transfer Catalysis http://chemlabs.princeton.edu/macmillan/wp-content/uploads/sites/6/AM_phase-transfer-catalysis.pdf (accessed Oct 1, 2017).

(177) Fong, D.; Bodnaryk, W. J.; Rice, N. A.; Saem, S.; Moran-Mirabal, J. M.; Adronov, A. *Chem. - A Eur. J.* **2016**, *22* (41), 14560–14566.

(178) CellScale. MicroSquisher Micro-scale Tension-Compression Test System https://cellscale.com/wp-content/uploads/2016/11/MicroSquisher-User-Manual-v3.5.pdf.

(179) Compression Testing of Soft Materials Compression of a Cylindrical Specimen http://cellscale.com/wp-content/uploads/2016/11/Compression-Testing-of-Soft-Materials.pdf (accessed Jan 10, 2018).

(180) Kim, K.; Cheng, J.; Liu, Q.; Wu, X. Y.; Sun, Y. *J. Biomed. Mater. Res. Part A* **2010**, *92A* (1), 103–113.

(181) Hodgson, S. M.; Bakaic, E.; Stewart, S. A.; Hoare, T.; Adronov, A. *Biomacromolecules* **2016**, *17* (3), 1093–1100.

(182) Long, R.; Hall, M. S.; Wu, M.; Hui, C.-Y. *Biophys. J.* **2011**, *101* (3), 643–650.

(183) Anseth, K. S.; Bowman, C. N.; Brannon-Peppas, L. *Biomaterials*. Elsevier January 1, 1996, pp 1647–1657.

(184) Takigawa, T.; Morino, Y.; Urayama, K.; Masuda, T. *Polym. Gels Networks* **1996**, *4* (1), 1–5.

(185) Ling, I.; Alias, Y.; Makha, M.; Raston, C. L. *New J. Chem.* **2009**, *33* (7), 1583–1587.

(186) Dionisio, M.; Schnorr, J. M.; Michaelis, V. K.; Griffin, R. G.; Swager, T. M.; Dalcanale, E. *J. Am. Chem. Soc.* **2012**, *134* (15), 6540–6543.

(187) Lobach, A. S.; Ryzhkina, I. S.; Spitsina, N. G.; Obraztsova, E. D. In *Physica Status Solidi (B) Basic Research*; Wiley-Blackwell, 2007; Vol. 244, pp 4030–4034.

Appendix A: General Experimental

All reagents were obtained from commercial sources and were used as received without further purification. Raw HiPCO SWNTs were purchased from NanoIntegris (batch #HR27-104, 10 wt % in anhydrous EtOH) and used without further purification. Flash chromatography was performed using an IntelliFlash 280 system from Analogix. Unless otherwise noted, compounds were monitored using a variable wavelength detector at 254 nm. Solvent amounts used for gradient or isocratic elution were reported in column volumes (CV). Columns were prepared in Biotage® SNAP KP-Sil cartridges using $40 - 63$ µm silica or $25 - 40$ µm silica purchased from Silicycle. ^{1}H-NMR spectra of small molecules and polymers were recorded on Bruker Avance 600 MHz and 700 MHz spectrometers respectively. Polymer molecular weights and dispersities were analyzed (relative to polystyrene standards) *via* GPC using a Waters 2695 Separations Module equipped with a Waters 2414 refractive index detector and a Jordi Fluorinated DVB mixed bed column in series with a Jordi Fluorinated DVB 10^5 Å pore size column. THF with 2% acetonitrile was used as the eluent at a flow rate of 2.0 mL/min. Sonication was performed in a Branson Ultrasonic B2800 bath sonicator. Centrifugation of the polymer-SWNT samples was performed using a Beckman Coulter Allegra X-22 centrifuge. UV-Vis-NIR spectra were recorded on a Cary 5000 spectrometer in dual beam mode, using matching 10 mm quartz cuvettes. Thermogravimetric analysis was performed on a Mettler Toledo TGA/DSC 3+, and all measurements were conducted under an argon atmosphere, with sample masses ranging from 0.5 to 1.0 mg. Raman spectra were collected using a Renishaw InVia Laser Raman spectrometer, with three different lasers: a 25 mW argon ion laser (514

nm, 1800 L/mm grating); a 500 mW HeNe Renishaw laser (633 nm, 1800 L/mm grating); and a 300 mW Renishaw laser (785 nm, 1200 L/mm grating). For the raw SWNT sample dispersed in $CHCl_3$, laser intensity was set to 1% for 514 nm and 633 nm, and 10% for 785 nm. For the polymer-SWNT samples, laser intensity was set to 1% for all excitation wavelengths. Fluorescence spectra were measured on a Jobin-Yvon SPEX Fluorolog 3.22 equipped with a 450 W Xe arc lamp, digital photon counting photomultiplier, and an InGaAs detector, also using a 10 mm quartz cuvette. Slit widths for both excitation and emission were set to 10 nm band-pass, and correction factor files were applied to account to instrument variations. Photoluminescence maps were obtained at 25 °C, with 5 nm intervals for both the excitation and emission.

Appendix B: Synthetic Procedures
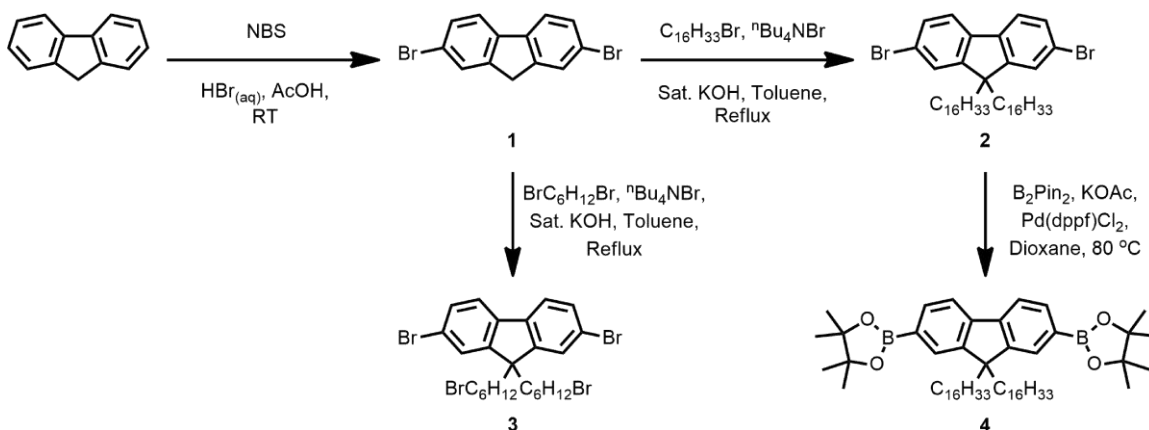
Scheme S1. Synthesis of monomers **3** and **4**.

2,7-dibromofluorene (1) (prepared according to literature procedures[146])

A round bottom flask equipped with a magnetic stir bar was charged with fluorene (33.2 g, 200 mmol), NBS (89.0 g, 500 mmol) and acetic acid (400 mL). While the mixture was stirring, conc. HBr (10 mL) was slowly added and then the reaction mixture was stirred at RT for 1.5 h. Water (200 mL) was added and the resulting suspension was filtered and washed with water to obtain an orange-white solid. The solid was recrystallized from a 1.5:1 v/v mixture of EtOH:acetone (~1.8 L total volume), and the mother liquor was recrystallized again from the same solvent mixture (~1.5 L total volume). The crops were combined to afford **1** (41.2 g, 64%) as a colourless solid. ^{1}H-NMR (600 MHz; CDCl$_3$): δ 7.67 (d, J = 1.1 Hz, 2H), 7.61 (d, J = 8.1 Hz, 2H), 7.51 (dd, J = 8.1, 1.8 Hz, 2H), 3.88 (s, 2H).

2,7-dibromo-9,9-dihexadecylfluorene (2) (prepared according to literature procedures[146])

A round bottom flask equipped with a magnetic stir bar was charged with **1** (2.7 g, 8.3 mmol), 1-bromohexadecane (6.36 g, 20.8 mmol), $^nBu_4NBr$ (537 mg, 1.7 mmol), toluene (16.6 mL), and sat. KOH (aq) (16.6 mL). The reaction mixture was heated to 60 °C and stirred vigorously for 1 h under a nitrogen atmosphere. The biphasic mixture was allowed to separate, and the organic layer was isolated. The aqueous phase was extracted twice with diethyl ether (2 x 20 mL) and the organic extracts were combined and concentrated *in vacuo* to obtain a viscous green oil. The crude product was purified by flash chromatography (100 g column, 100% hexanes over 10 CV) to afford **2** as a colourless solid (5.19 g, 81%). ^{1}H-NMR (600 MHz; CDCl$_3$): δ 7.51 (d, $J = 8.0$ Hz, 1H), 7.46-7.43 (m, 2H), 1.92-1.88 (m, 2H), 1.24-1.03 (m, 26H), 0.88 (t, $J = 7.0$ Hz, 3H), 0.59-0.57 (m, 2H).

2,7-dibromo-9,9-bis(6-bromohexyl)fluorene (3) (prepared according to literature procedures[146])

A round bottom flask equipped with a magnetic stir bar was charged with **1** (5 g, 15.4 mmol), 1,6-dibromohexane (37.7 g, 154 mmol), toluene (31 mL), and sat. KOH (31 mL). $^nBu_4NBr$ (1.0 g, 3.1 mmol) was then added and the reaction mixture was heated to 60 °C and stirred vigorously for 1 h under a nitrogen atmosphere. The biphasic mixture was allowed to separate, and the organic layer was isolated. The aqueous phase was extracted twice with diethyl ether (2 x 120 mL) and the organic extracts were combined and concentrated *in vacuo* to obtain a viscous green oil. Excess 1,6-dibromohexane was removed using vacuum distillation (1 mbar, 115 °C) to obtain a viscous yellow oil. The crude mixture was purified by flash chromatography (100 g column, 0 to 20% CH$_2$Cl$_2$ in

hexanes over 10 CV) to obtain a colourless solid containing two spots by TLC. The crude product was recrystallized from MeOH (~250 mL) to afford **3** as a colourless solid (4.4 g, 44%). ^{1}H-NMR (600 MHz; CDCl$_3$): δ 7.53-7.52 (m, 1H), 7.47-7.43 (m, 2H), 3.31-3.28 (t, 2H), 1.94-1.91 (m, 2H), 1.68-1.66 (m, 2H), 1.22-1.19 (m, 2H), 1.10-1.07 (m, 2H), 0.60-0.57 (m, 2H).

2,2'-(9,9-dihexadecylfluorene-2,7-diyl)bis(4,4,5,5-tetramethyl-1,3,2-dioxaborolane) (4) (prepared according to literature procedures[146])

A round bottom flask equipped with a magnetic stir bar was charged with **2** (5.2 g, 6.7 mmol), B$_2$Pin$_2$ (3.76 g, 14.8 mmol), KOAc (1.98 g, 20.2 mmol), and dioxane (28 mL). Pd(dppf)$_2$Cl$_2$ (165 mg, 202 µmol) was added and then the reaction mixture was stirred at 80 °C for 12 h. The reaction mixture was partitioned with water and extracted thrice with Et$_2$O. The organic extracts were combined and dry loaded onto silica (9.9 g). The crude product was purified by flash chromatography (100 g column, 0 to 70% CH$_2$Cl$_2$ in hexanes over 10 CV) to afford **3** as a colourless solid (4.88 g, 63%). ^{1}H-NMR (600 MHz; CDCl$_3$): δ 7.80 (d, J = 7.5 Hz, 1H), 7.74-7.71 (m, 2H), 2.00-1.97 (m, 2H), 1.39 (s, 12H), 1.24-0.99 (m, 26H), 0.87 (t, J = 7.0 Hz, 3H), 0.55-0.53 (m, 2H).
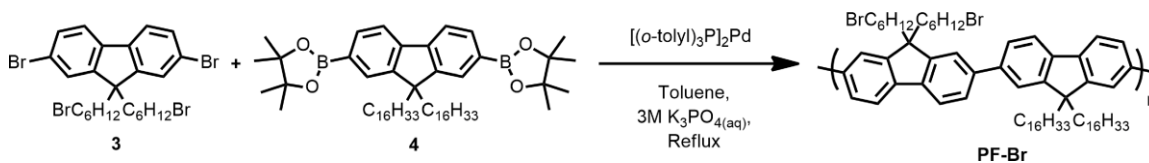
Scheme S2. Synthesis of **PF-Br**.

Poly(dihexadecylfluorene-alt-bis(bromohexyl)fluorene) (PF-Br) (prepared according to literature procedures[146])

A Schlenk tube equipped with a magnetic stir bar was charged with **3** (1.50 g, 1.73 mmol), **4** (1.13 g, 1.73 mmol), toluene (12.4 mL), and 3M K_3PO_4(aq) (12.4 mL). The biphasic mixture was degassed by three freeze pump-thaw cycles, then, while frozen under liquid nitrogen, [(o-tol)$_3$P]$_2$Pd (62 mg, 87 µmol) was added under a positive pressure of nitrogen. The Schlenk tube was evacuated and backfilled with nitrogen four times, and the reaction mixture was vigorously stirred at 80 °C for 12 h. The phases were allowed to separate, and the organic layer was isolated and filtered through a single plug of celite and neutral alumina. The plug was thoroughly washed with THF and the flow-through was concentrated *in vacuo*. The crude polymer was precipitated into MeOH (400 mL) and then filtered to afford **PF-Br** as a yellow solid (1.71 g, 89%). ^{1}H-NMR (700 MHz; CDCl$_3$): δ 7.85-7.83 (m, 4H), 7.73-7.68 (m, 8H), 3.30 (t, 4H), 2.17-2.11 (m, 4H), 1.72-1.69 (m, 4H), 1.30-1.13 (m, 60H), 0.87 (t, 6H). GPC: M_n = 31 kDa, Đ = 2.02.
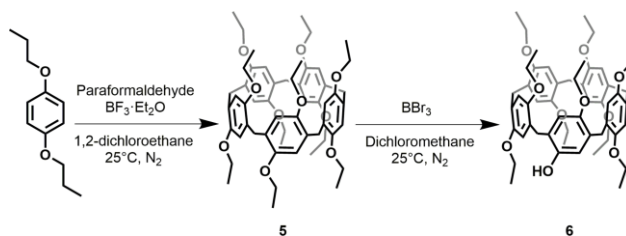
**Scheme S3.** Synthesis of mono-de-ethylated pillar[5]arene (**6**).

1,4-bis(ethoxy)pillar[5]arene (5) (adapted from literature procedures[166])

A round bottom flask equipped with a magnetic stir bar was charged with 1,4-diethoxybenzene (10 g, 60 mmol), paraformaldehyde (5.42 g, 180.6 mmol), and 1,2-dichloroethane (130 mL). BF$_3$·Et$_2$O (7.43 mL, 60.2 mmol) was added dropwise to the

reaction mixture at RT under a nitrogen atmosphere. The mixture was stirred for 1 h at RT before diluting with hexanes (200 mL) and filtering through a silica plug and washing with 50/50 v/v CH_2Cl_2:hexanes. Fractions containing pillar[5]arene **5** (R_f ~0.5, 70/30 CH_2Cl_2:hexanes) were concentrated *in vacuo* to afford **5** as a colourless solid (4.3 g, 40%). ^{1}H-NMR (600 MHz; $CDCl_3$): δ 6.82 (s, 10H), 3.88 (q, $J = 7.0$ Hz, 20H), 3.77 (s, 10H), 1.36 (t, $J = 7.0$ Hz, 30H).

Mono-de-ethylated Pillar[5]arene (6) (adapted literature procedures[166])

A 500 mL flame-dried round bottom flask equipped with a magnetic stir bar was charged with **5** (1 g, 1.12 mmol) and CH_2Cl_2 (120 mL). A BBr_3 solution (1M in CH_2Cl_2; 1.0 mL, 1 mmol) was added dropwise to the reaction mixture at RT under a nitrogen atmosphere. The mixture was stirred for 20 min at RT before quenching the reaction with dH_2O (~10 mL). The organic phase was extracted with brine, dried with $MgSO_4$, and concentrated *in vacuo*. The crude product was purified by flash chromatography (100 g column, 5 to 10% EtOAc in hexanes over 10 CV; monitored at 296 nm) to afford **6** as a colourless solid (194 mg, 20%). ^{1}H-NMR (600 MHz; $CDCl_3$): δ 6.90 (s, 1H), 6.78 (s, 1H), 6.70 (s, 1H), 6.69 (s, 1H) 6.64 (m, 3H), 6.55 (m, 3H), 6.49 (s, 1H), 4.03 (q, $J = 7.0$ Hz, 2H), 3.92-3.72 (m, 24H), 3.64 (q, J = 7.0 Hz, 2H), 1.44-1.35 (m, 10H), 1.24-1.07 (m, 16H), 1.03 (t, $J = 7.0$ Hz, 3H).

Scheme S4. Synthesis of **PF-Pillar**.
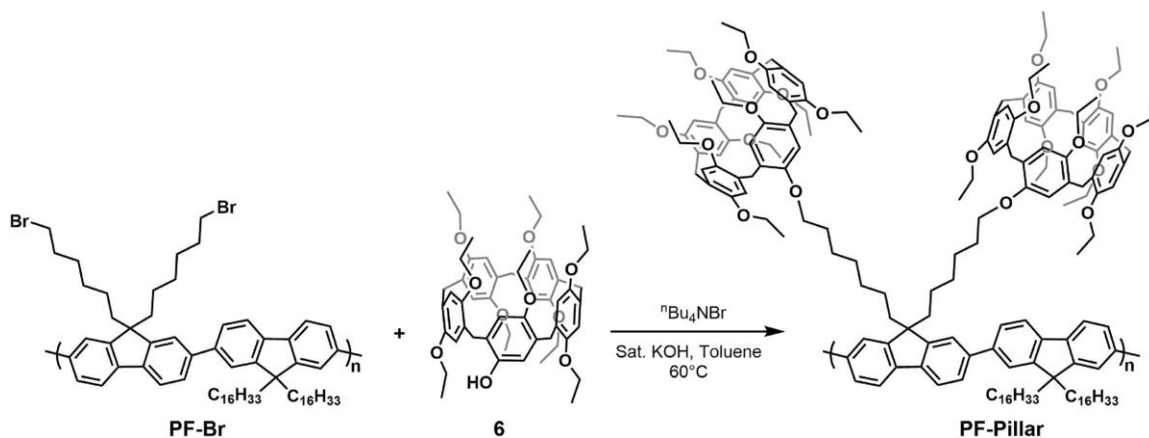
Poly(dihexadecylfluorene-*alt*-bis(pillar[5]arene)fluorene) (PF-Pillar)

A round bottom flask equipped with a magnetic stir bar was charged with **PF-Br** (50 mg, 45 µmol), **6** (97.8 mg, 110 µmol), $^{n}Bu_4NBr$ (5.8 mg, 20 µmol), toluene (400 uL) and sat. KOH (400 uL). The reaction mixture was stirred for 12 h at 60°C. The reaction mixture was cooled to RT, filtered through an alumina plug and precipitated into MeOH (~20 mL). The suspension was filtered and dried by vacuum to afford **PF-Pillar** as a yellow solid (61 mg, 50%). ^{1}H-NMR (700 MHz; CDCl$_3$): δ 7.87-7.69 (m, 12H), 6.78-6.66 (m, 20H), 3.84-3.63 (m, 60H), 2.21-2.13 (m, 7H), 1.56-1.13 (m, 90H).

Appendix C: Calculations and Figures

Calculation of SWNT Concentration by TGA

The relevant data to calculate SWNT concentration are tabulated in Table S1. The mass losses, which correspond to polymer side chain degradation, were used to calculate the SWNT mass fraction (f_{SWNT}). Given that the SWNT mass loss is negligible under the experimental conditions, the mass fraction of the polymer ($f_{polymer}$) can be calculated according to Eq. S1:

$$f_{polymer} = \frac{\varphi_{polymer-SWNT}}{\varphi_{polymer}} \qquad (S1)$$

Where $\varphi_{polymer}$ is the mass loss of polymer and $\varphi_{polymer-SWNT}$ is the mass loss of the polymer-SWNT complex. f_{SWNT} can then be calculated accordingly, given that $f_{polymer} + f_{SWNT} = 1$. For the **PF-Pillar**-SWNT dispersion, $V_{polymer-SWNT}$ was 0.5 mL, $m_{polymer-SWNT}$ was 0.5 mg, and f_{SWNT} was 0.60. The SWNT concentration (c_{SWNT}) was calculated according to Eq. S2:
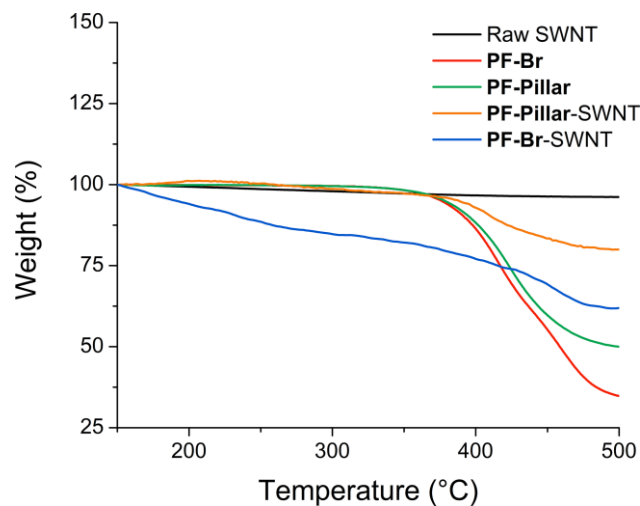
$$c_{SWNT} = \frac{f_{SWNT} \times m_{polymer-SWNT}}{V_{polymer-SWNT}} \qquad (S2)$$

$$c_{SWNT} = \frac{0.6 \times 0.5\ mg}{0.5\ mL}$$

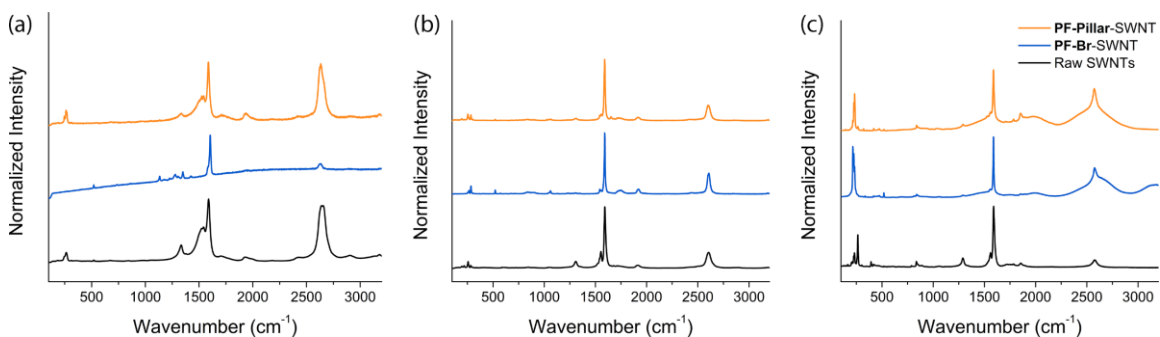$$c_{SWNT} = 600\ \mu g \cdot mL^{-1}$$

Table S1. Tabulated Data for SWNT Concentration Calculations.

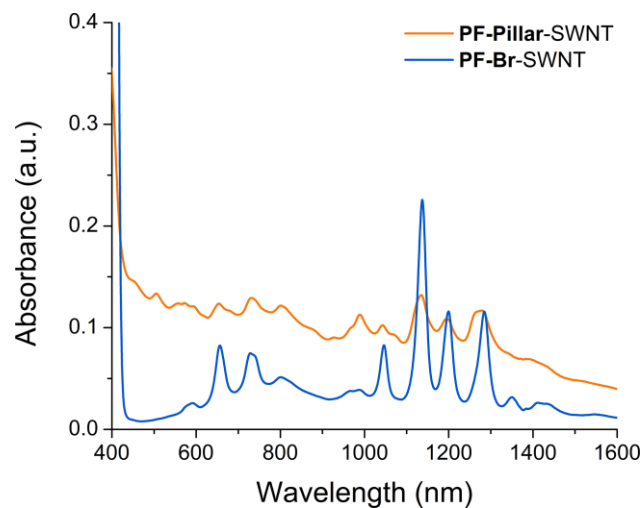|	PF-Br	PF-Pillar
$\varphi_{polymer}$	65.2%	50.1%
$\varphi_{polymer-SWNT}$	38.1%	20.1%
f_{SWNT}	0.42	0.60
$V_{polymer-SWNT}$	6 mL	0.5 mL
$m_{polymer-SWNT}$	0.3 mg	0.5 mg

Figure S1. TGA thermograms of **PF-Pillar** (green), **PF-Br** (red), **PF-Pillar**-SWNT (orange), **PF-Br**-SWNT (blue), and Raw HiPCO SWNTs (black).
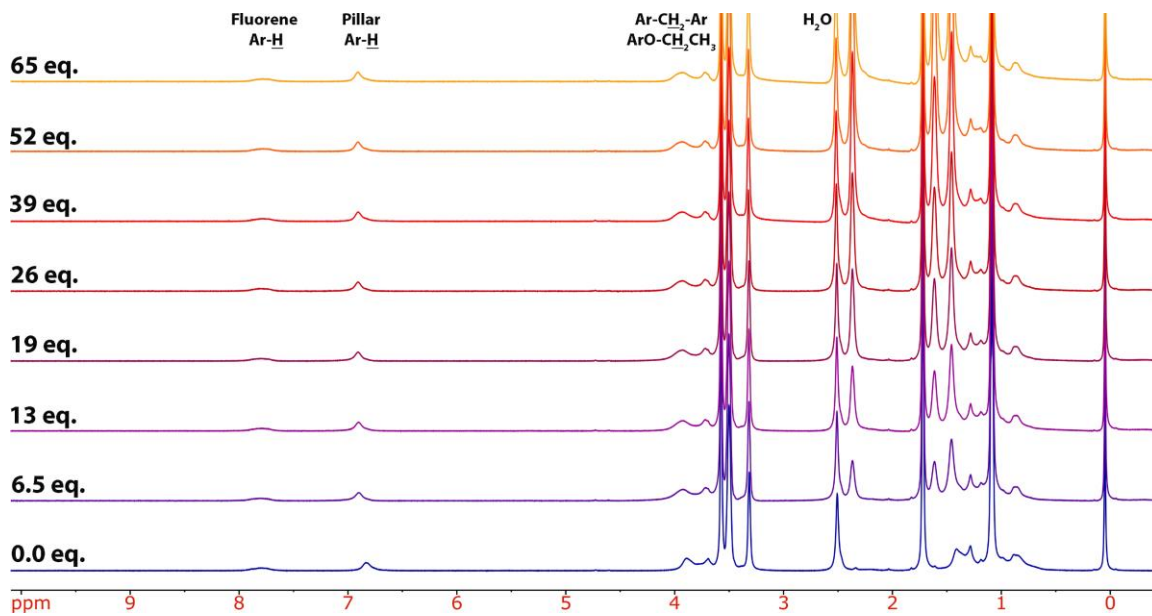

Figure S2. Full Raman spectra of raw HiPCO and polymer-SWNT samples at (a) 514, (b) 633, and (c) 785 nm excitation wavelengths. The spectra were normalized to the G-band at ~1590 cm-1 and offset for clarity.
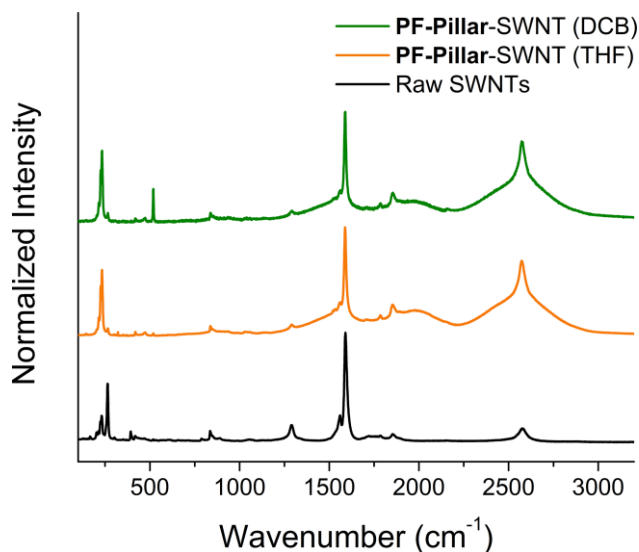
Figure S3. UV-Vis-NIR spectra of **PF-Pillar**-SWNT (orange) and **PF-Br**-SWNT (blue) used for PL mapping.
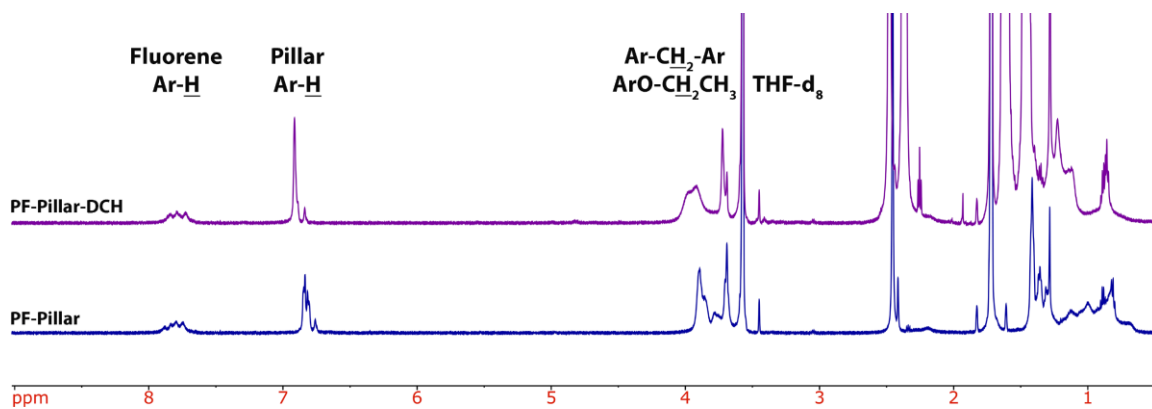
Figure S4. ^{1}H-NMR spectra (THF-d8, 298 K) of **PF-Pillar** (blue) recorded after the addition of 78 eq of 1,6-dicyanohexane (DCH; purple).

Figure S5. Full ^{1}H-NMR spectra (THF-d8, 298 K) of the **PF-Pillar**-SWNT dispersion recorded after successive additions of 1,6-dicyanohexane (0 – 65 eq).

Figure S6. Full Raman spectra of **PF-Pillar**-SWNT samples in THF and upon solvent exchange into 1,2-dichlorobenzene (DCB), compared with raw HiPCO SWNTs. The spectra were collected at 785 nm excitation wavelength, normalized to the G-band at ~1590 cm-1 and offset for clarity.